crystals

MDPI

Article

Improving Weld Stability in Gas Metal Arc Welding: A Data-Driven and Machine Learning Approach

Elina Mylen Montero Puñales [1,*], Guillermo Alvarez Bestard [2] and Sadek Crisóstomo Absi Alfaro [3]

[1] Department of Mechanical, Mechatronic Engineering, Faculty of Technology, University of Brasilia, Brasilia 70910-900, DF, Brazil
[2] Faculty Engineering, University of Brasilia, Campus Gama, Brasilia 70910-900, DF, Brazil; guillermo@unb.br
[3] Department of Mechanical, Mechatronic Engineering, Faculty of Technology, University of Brasilia, Campus Universitario Darcy Ribeiro, Brasilia 70910-900, DF, Brazil; sadek@unb.br
* Correspondence: mylen88a@gmail.com

Abstract

The Gas Metal Arc Welding (GMAW) process is widely utilized in industrial production, requiring careful selection of appropriate procedures to ensure the highest quality. A key area of study closely related to GMAW quality is the control of process stability. This research presents a methodology for analyzing welding data to identify instability, thus enabling the development of a stability indicator. Our approach focuses on sensory fusion by integrating multiple sources of information, including sound signals, images, and current signals captured during the welding process. This work explores various configurations of variables to analyze the three primary transfer modes. Additionally, a comprehensive statistical analysis of the results obtained is conducted. Image processing techniques, sound analysis, and artificial intelligence methodologies are employed to enhance the analysis process.

Keywords: GMAW; quality index; GMAW process stability

check for updates

Academic Editor: Shouxun Ji

Received: 7 March 2025
Revised: 26 March 2025
Accepted: 27 March 2025
Published: 16 October 2025

Citation: Puñales, E.M.M.; Bestard, G.A.; Alfaro, S.C.A. Improving Weld Stability in Gas Metal Arc Welding: A Data-Driven and Machine Learning Approach. *Crystals* **2025**, *15*, 895. https://doi.org/10.3390/cryst15100895

Copyright: © 2025 by the authors. Licensee MDPI, Basel, Switzerland. This article is an open access article distributed under the terms and conditions of the Creative Commons Attribution (CC BY) license (https://creativecommons.org/licenses/by/4.0/).

1. Introduction

Gas Metal Arc Welding (GMAW) is a widely employed welding process known for its production efficiency, reliability, and automation capabilities. It involves creating an arc between a continuously fed consumable electrode, a shielding gas, and the workpiece. GMAW can be categorized as Metal Active Gas (MAG) or Metal Inert Gas (MIG), depending on the type of gas used. With proper parameter configuration, it enables welding in various positions and with a wide range of metal alloys. However, due to the inherent complexity of the process, achieving consistent quality requires careful procedure selection.

Process stability is a critical aspect directly linked to welding quality, encompassing factors such as metallic transfer regularity, arc stability, and operational behavior. A stable arc in GMAW results in a more stable welding process and improved weld quality, characterized by enhanced penetration and reduced spatter. Metal transfer, which is influenced by parameters like current, voltage, electrode diameter, and shielding gas composition, significantly impacts both arc stability and the final weld bead's geometry. Additionally, operational behavior and parameter settings play a substantial role in determining stability. Factors such as arc length, wire feed speed, and voltage influence process stability, demanding careful optimization.

Understanding and controlling these variables are crucial in ensuring high-quality welds in GMAW. This research proposes a methodology for analyzing welding data using a

sensory fusion approach, incorporating sound signals, images, and current signals acquired during the welding process. By conducting detailed statistical analysis and employing image processing techniques, sound analysis, and artificial intelligence, this study aims to develop a stability indicator that identifies and evaluates process instability. The proposed approach has the potential to enhance process control, leading to improved welding quality and greater efficiency in industrial applications.

Signal analysis using probabilistic models and algorithms has been widely explored in understanding stochastic processes and their behavior during disturbances. Previous studies, such as that by Adolfsson and Bahrami [1], focused on the statistical treatment of electrical signals during welding disruptions. They found that the instability of the welding process correlates with a decrease in the variance of weld voltage and a reduced short-circuit transfer rate. However, no significant decrease was observed in the estimated variance of welding current. Similarly, Luksa [2] investigated disturbances caused by external factors, such as grease and paint affecting the gas shield, and variations in wire extension. Parameters such as the mean, variance of welding current, time of arc burning, and short-circuit frequency were calculated to identify these disturbances.

In summary, statistical parameters play a crucial role in describing the dynamic and stochastic characteristics of the welding process. The mean reflects the general amplitude of the measured variable, while the standard deviation indicates the difference between the value of a stochastic variable and its expected value. Kurtosis provides insight into the sharpness or smoothness of the data distribution, relative to a Gaussian distribution. By combining these statistical parameters, a comprehensive understanding of the specific welding process's behavior can be achieved.

Mousavi and Haeri (2011) [3] demonstrated a relationship between droplet detachment and statistical parameters of current, highlighting that uniform droplet detachment and arc length uniformity are indicated by a lower standard deviation and coefficient of variation. Image processing, laser shadowing, and sound processing techniques are commonly used to measure these variables. Proper control ensures the appropriate transfer mode, leading to improved welding quality and reduced defects. The authors emphasized that large drops do not represent favorable conditions.

Suban [4] emphasized the importance of maintaining a consistent time interval between the transfer of subsequent drops to maximize stability. This criterion contributes to achieving a more stable short-circuit material transfer.

Different transfer modes (open arc, short circuit, and spray) were identified based on the type of gas used. Probability distribution analysis of voltage and current using Fourier analysis was performed, with the authors concluding that pure CO_2 leads to greater stability. This method is simple and feasible for real-time implementation.

The acoustic signal contains valuable information about the transfer mode, arc behavior, changes in arc dimensions and geometry, arc intensity variations, metal transfer, and molten pool oscillations. Mota et al. [5] demonstrated that electrical and acoustic signals are highly correlated, especially in the short-circuit transfer mode, allowing for the identification of drop detachment and arc reignition. This method is cost-effective and suitable for industrial implementation.

Combining these methods with machine learning techniques has become essential for monitoring and controlling welding processes. Artificial neural networks are widely used to evaluate stability, predict bead geometry, select the most appropriate shielding gas, and detect weld defects in real time. Regression models, genetic algorithms, and fuzzy logic are also extensively applied to determine optimal GMAW process parameters.

Kim et al. [6] identified neural networks as highly suitable for predicting weld bead geometry and mechanical properties. Their learning capacity allows for the development

of efficient models by considering the stochastic nature of the process and the variables involved, enabling effective mapping of the parameter relationships.

Considering the concepts mentioned above, this study integrates statistical methods, image processing algorithms, and machine learning techniques to monitor stability in the GMAW process.

2. Materials and Methods

This chapter outlines the methods and tools employed in this study. The initial stage focuses on the acquisition and analysis of data from various sources and sensors. A comprehensive range of data was collected to ensure a holistic understanding of the GMAW welding process. These data sources include sound signals, images, and current signals captured during the welding process. Thorough analysis and preprocessing techniques were applied to ensure data quality and reliability.

Subsequently, the collected data were integrated and correlated to reveal meaningful relationships and insights. This integration process allows for a comprehensive examination of the multiple factors that influence the stability and quality of the welding process. By combining different data sources, a more accurate representation of the process dynamics can be achieved.

In the final step, machine learning algorithms were employed to process the integrated data. These algorithms play a crucial role in identifying patterns and extracting valuable information from the dataset. Through extensive training and analysis, machine learning models can recognize stability rules and indicators within the GMAW welding process. These findings form the foundation for developing a stability and quality indicator, which serves as a valuable tool for monitoring and improving the welding process.

The methods and tools utilized in this study provide a systematic and data-driven approach to understanding and enhancing the GMAW welding process. The integration of data from various sources, coupled with advanced machine learning techniques, enables a comprehensive analysis of the process dynamics, ultimately leading to improved stability and quality control.

2.1. Data Acquisition System

Figure 1 shows the layout of the computer system and the hardware used in this research. The next section provides a brief description of each device, its function, and the materials involved in the process.

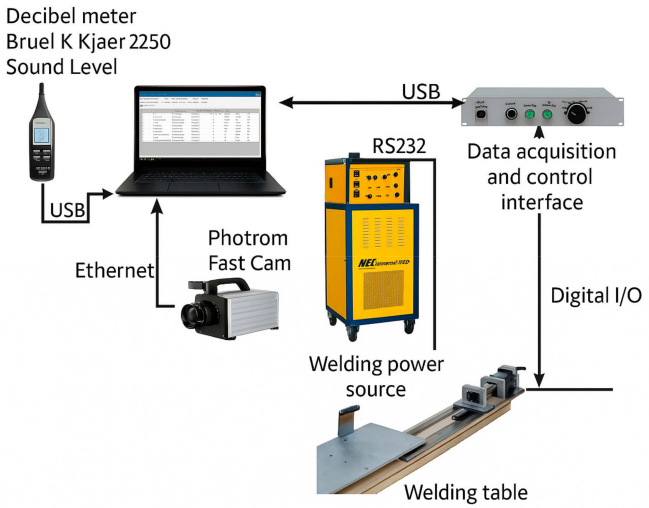


Figure 1. Data acquisition system: main components, welding table, and instrument support.

2.1.1. Welding Power Source

The Inversal 450 welding power source (IMC Soldagem, São Paulo, Brazil) is equipped with an RS232 interface for reading operation parameters. It enables the acquisition of effective welding voltage and electric current values with a sampling time of 2 ms or less. The measurement system's analog-to-digital converter has 10 bits, providing a resolution of 0.07 V for welding voltage and 0.44 A for welding electric current. The control interface, developed by GRACO (University of Brasília—UnB, Brazil), includes a stepper motor driver for workpiece movement, and the welding speed is obtained directly from the interface registers via USB connection.

2.1.2. Flat Welding Table

The electromechanical system used for moving the workpiece consists of a linear axis with 5 mm movement per revolution and a stepper motor with 1.8 degrees per step. Developed by GRACO students (University of Brasília—UnB, Brazil), it incorporates a stepper motor controller circuit with signals for adjusting speed and direction. The system can handle a maximum load of 15 kg and achieve a maximum speed of 15 mm/s. The movement system is controlled via digital I/O from the main interface unit.

2.1.3. Process Consumables

According to the availability of the laboratory, the materials used in this research were as follows: The GMAW process under study utilized a gas shield composed of 96% Ar and 4% CO_2. The gas flow rate during the experiment was set to 15 lt/min. For weld bead modeling and reinforcement, a solid wire of AWS A5.18 ER70S class with a diameter of 1 mm was used.

2.1.4. User Interface

The user interface system, also developed by GRACO students (University of Brasília—UnB, Brazil) [7], facilitates the creation of welding sequences. It allows for defining start and end positions, stimuli to be sent to the welding power source, and the sampling period. The interface communicates with the system via USB and RS232. The process starts automatically and stops upon sequence completion or manual intervention. The sampling time is set to 20 ms, generating three files per experiment to store system configuration, stimulus sequences, and collected measurements. The software version used was the latest internal version developed by GRACO in 2017.

2.1.5. Sound Level Meter

The sound pressure is a result of sound propagation, created by the energy of sound waves causing air particles to move and alternating the static pressure of the air. These pressure variations occur in areas of particle concentration (concentration zones) and areas with lower saturation (refractive zones). The acoustic pressure is defined as the instantaneous pressure difference from static atmospheric pressure. It is measured in Pascals and originates from longitudinal or transverse mechanical variations. The human ear can perceive sound when these variations are longitudinal and range from 20 Hz to 20 kHz. To measure sound pressure, a microphone is used as a transducer that converts acoustic mechanical energy into an electrical signal. The microphone sensitivity represents the relationship between acoustic and electrical pressure variation.

The sound analysis presented in this study is based on previous investigations by a GRACO-UNB student [5]. Cayo and Alfaro [5] use sound to define the difference between the transfer modes in the GMAW process. They use sound pressure and current signals to identify changes in the transfer mode and identify defects. The Brüel & Kjær Type

2250 decibel meter (Brüel & Kjær, Nærum, Denmark) used in this project was connected via USB to the data processing system and uses Equation 1 for the calculation of acoustic pressure level, which will be referred to as sound pressure level (SPL) below.

In the context of this study, the following variables and parameters are defined:

SPL: Sound pressure level, which represents the level of acoustic pressure in the sound signal.

S: Amplitude of the sound signal over time.

P: Acoustic pressure, which is a factor influenced by geometric characteristics (experimentally determined as 10E = 5).

Po: Reference acoustic pressure, which is set to 20 uPa.

ξ: Integration time variable.

t: Start time of integration.

T: Integration time range.

These definitions provide a framework for understanding and analyzing the sound signal in terms of its pressure and amplitude over time. The SPL calculation involves considering the geometric factor (P), reference acoustic pressure (Po), integration time variable (ξ), start time (t), and integration time range (T). By incorporating these variables, researchers can measure and evaluate the sound pressure level (SPL) using the following equation:

$$SPL = 10 \times \log10[(P^2/Po^2) \times (\xi/T)] \quad (1)$$

To measure the weld bead geometry, images were captured from both vertical and horizontal angles. A Photoshop script was then used to measure the width and height at 1 mm intervals, after converting the pixel scale of the images into millimeters (as illustrated in Figure 2).

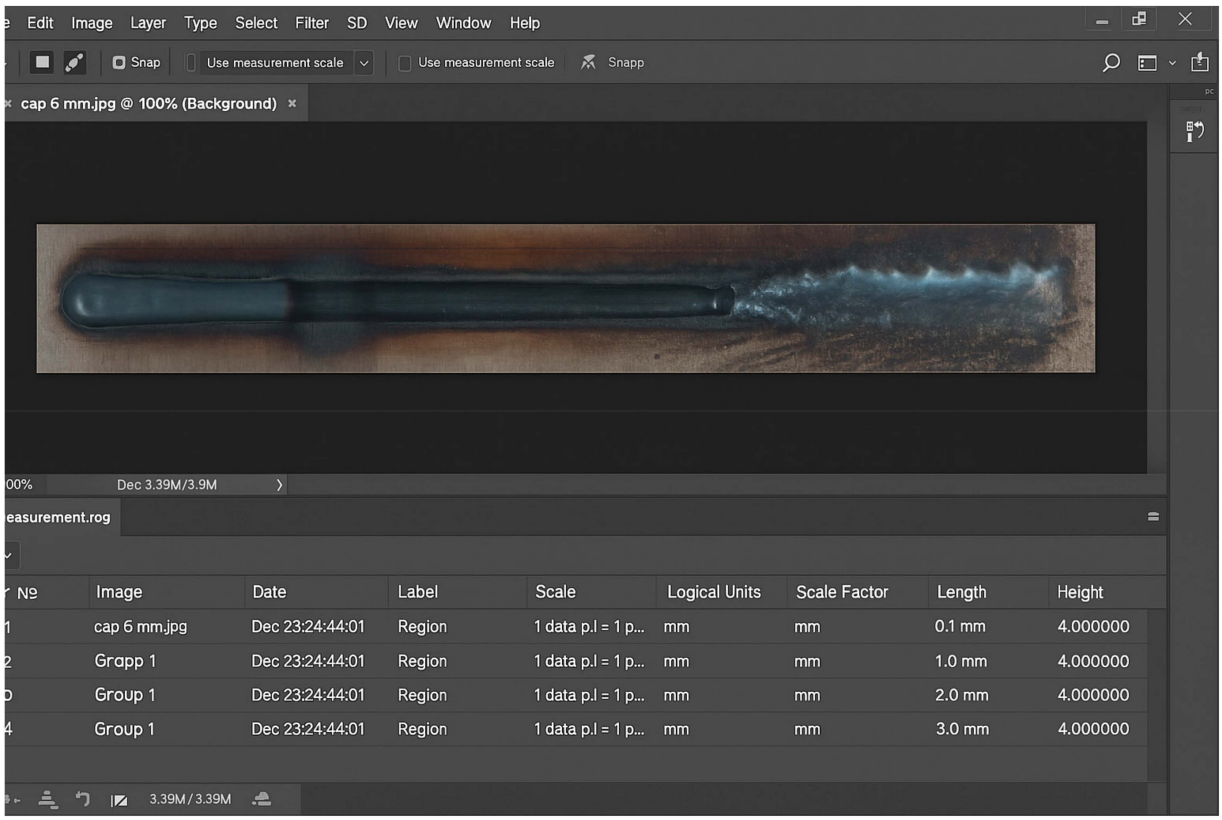


Figure 2. Weld bead dimensions' measurement.

2.2. Image Preprocessing

To capture the images, we employed the shadowgraph technique, which utilizes an optical expander composed of a divergent lens followed by a convergent lens (see Figure 3). The system operates with a He-Ne (Helium–Neon) laser as the light source. The divergent lens has a focal length of 40 mm, while the convergent lens collimates the laser beam, producing a consistent light path. The distance between the convergent lens and the welding wire is 70 cm, and the camera is positioned 40 cm from the wire.

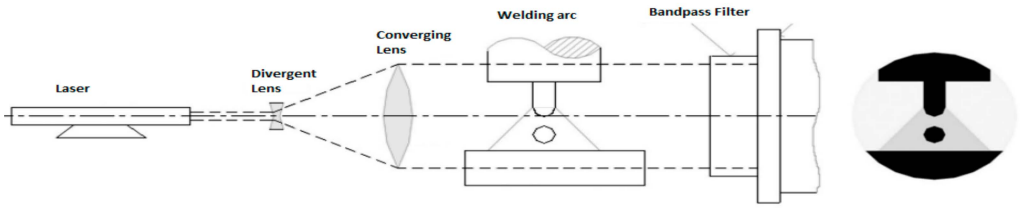


Figure 3. Assembly for application of shadowgraph technique (modified from [5]).

We used the Photron APX-RS high-frequency acquisition camera, which provides full-megapixel resolution images at frame rates of up to 3000 frames per second (fps). In the present work, the following configuration was used: a frame rate of 512 fps and a resolution of 512 × 512 pixels. The camera was operated using Photron FASTCAM Viewer (PFV) software, version 3.5. Figure 4 shows an example of an image obtained using the high-speed camera and profiling method.

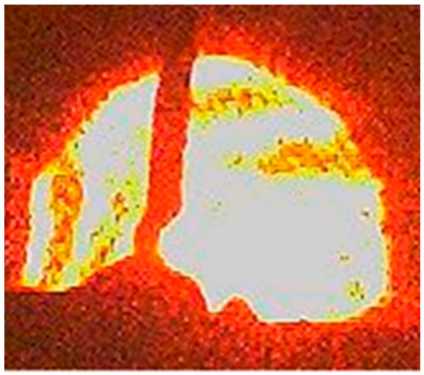


Figure 4. Example of an image obtained using the high-speed camera and profiling method.

The acquired data were transferred to the computer through an Ethernet connection. To process the data, a Python program (version 3.6) was developed using the OpenCV image processing library (OpenCV version 3.4). Each experiment's images underwent several computer vision techniques to enhance their quality and improve the effectiveness of subsequent processing steps. These techniques included the application of filters to reduce noise, isolate specific regions of interest, and perform image binarization. All operations were carried out directly on the pixel values in the spatial domain.

For smoothing, a Gaussian filter mask was applied. This linear filter helps reduce image noise and blurs the image by convolving it with the Gaussian kernel.

Similarly, a median filter was utilized to further soften the image. It replaces each pixel's value with the median of the grayscale values in its local neighborhood, determined by kernel size. This technique is effective in eliminating isolated pixels or small anomalies.

Finally, the images were subjected to thresholding segmentation, a technique for segmenting homogeneous regions based on similarity characteristics. Thresholding segmentation involves applying a specific grayscale threshold (T) to the image f(x,y) to transform it into a binary image g(x,y) with a clear distinction between objects of interest and the

background. The relation between the grayscale threshold and the image was used to determine the binary segmentation.

By employing these image processing techniques, the acquired images were enhanced, the noise was reduced, and the relevant regions were isolated, laying the foundation for subsequent analysis and interpretation.

Figure 5 shows an example of the results obtained using these techniques.

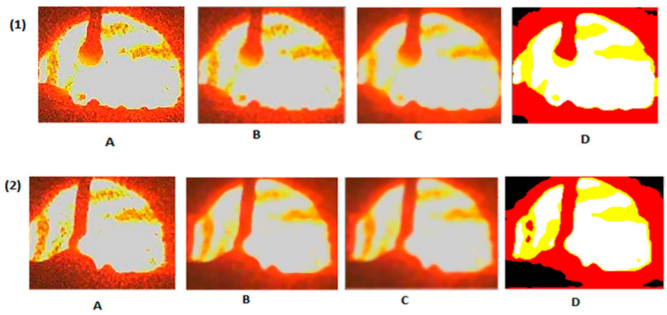


Figure 5. Image processing steps applied to two original frames.

Shows two original images:

(1) Sequence of transformations applied to the first image:

A′—Original image; B′—Image after applying median filter; C′—Image after applying Gaussian filter; D′—Binary image with color segmentation.

(2) Sequence of transformations applied to the second image:

A″—Original image; B″—Image after applying median filter; C″—Image after applying Gaussian filter; D″—Binary image with color segmentation.

2.2.1. Drop Detachment Frequency

The drop detachment frequency was calculated using the following steps:

1. The images were processed with the filters mentioned in Section 2.2.
2. Using the first image of the process, a square was marked in the area between the electrode and the piece to be welded.
3. For each image in the sequence, the number of pixels was counted, and the drop was identified based on the presence of red pixels.
4. We verified whether the drop appeared in more than one image to avoid counting it multiple times by mistake.A mathematical relationship was created between the number of images obtained per second and the number of drops obtained at that time.

The proposed method was tested for the three main transfer modes. To validate the effectiveness of the method, the current waveform was analyzed, and a manual analysis of the obtained images was conducted. Figure 6 illustrates an example of the processing performed, focusing on the desired area of the image. The presence of drops was analyzed in the subsequent three images. In this specific case, a short circuit was detected.

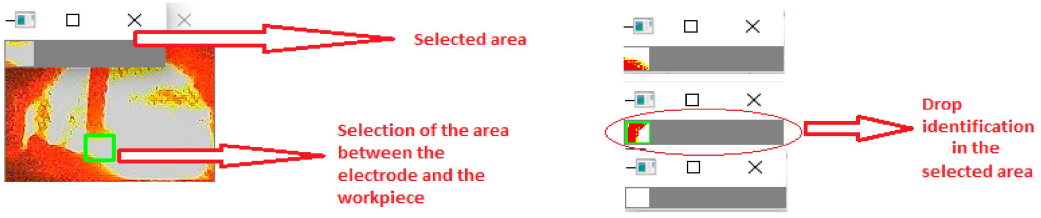


Figure 6. Identification of the drop detachment.

The green box indicates the region selected for drop detection in the Python-based image processing software. This area is located between the electrode and the workpiece. If the selected region was not blank—i.e., if it contained any red pixels—it was identified as a droplet event, as illustrated in the example on the right.

2.2.2. Identification of the Transfer Mode

For the definition of the transfer mode, a convolutional neural network that classifies the images between globular, spray, and short-circuit fundamental clusters was trained. The CNN processes input images and utilizes mathematical operations with kernels (filters) to create feature maps for each convolution. This enables the network to learn and recognize specific characteristics associated with each transfer mode, namely globular, spray, and short circuit.

The first convolutional layer consisted of 32 filters, while the second layer had 64 filters. The size of the filters used was 3×3 for the first layer and 2×2 for the second layer. After each convolutional layer, pooling was applied with a filter size of 2×2 to downsample the feature maps.

The CNN utilized a learning rate (lr) of 0.0004 to adjust its internal parameters (subsampling). By adjusting these parameters during training, the CNN learned to recognize and classify the distinct transfer modes based on the extracted features. The resulting trained CNN was then capable of accurately classifying new images into the appropriate transfer modes.

3. Results

The results obtained for each experiment are presented below. The experiments were performed by changing the values of the input parameters to study the influence and dependence of those parameters on the resulting welding geometry. The acquisition frequency of current signals is 20 ms and for sound signals, it is 100 ms due to the configuration available in the equipment used.

To conduct a comprehensive statistical analysis, the collected data were divided into sections. Each section corresponds to a specific set of input parameters, ensuring stability within that range. When the input parameters changed, a new section was studied independently, enabling the analysis of output parameter variations.

For the welding data, statistical values including the mean, standard deviation, peak value, and background value were calculated at intervals of 200 ms. Similarly, for the sound data, these statistical values were calculated at intervals of 100 ms. The analysis of these statistical values provided deeper insight into the variations and characteristics of the welding and sound data.

Statistical analysis of the data involved calculating specific parameters. The background welding current (bkg) was determined as the average of all current transient samples that were less than or equal to the mean current (A_mean). Similarly, the background welding voltage (bkg) was calculated as the average of all voltage transient samples that were less than or equal to the mean voltage (V_mean). On the other hand, the peak welding current (pkv) represented the average of all current samples greater than A_mean, and the peak welding voltage (pkv) was the average of all voltage samples greater than V_mean. The time registers of the data were used to synchronize both signals according to the welded position.

Welding was performed along the sheet metal from 5 mm to 180 mm, with a fixed contact tip-to-workpiece distance of 18 mm.

3.1. Results Obtained for Tests

In the first experiment, the welding speed value remained constant, while the wire feed speed and voltage varied. In the second experiment, high voltage values were utilized to achieve the globular and spray transfer modes, with the wire feed speed also being increased. Experiment three involved systematically increasing and then decreasing the voltage and wire feed speed to model the structural differences in deposition and observe the resulting changes in geometry. Lastly, experiment four aimed to analyze the influence of increased voltage and welding speed on the welding process.

The conducted experiments revealed a direct correlation between voltage and current values, as demonstrated in Experiment 1. Increasing the voltage led to a rise in current values (as shown in Figures 7 and 8), resulting in a greater deposition of material on the workpiece.

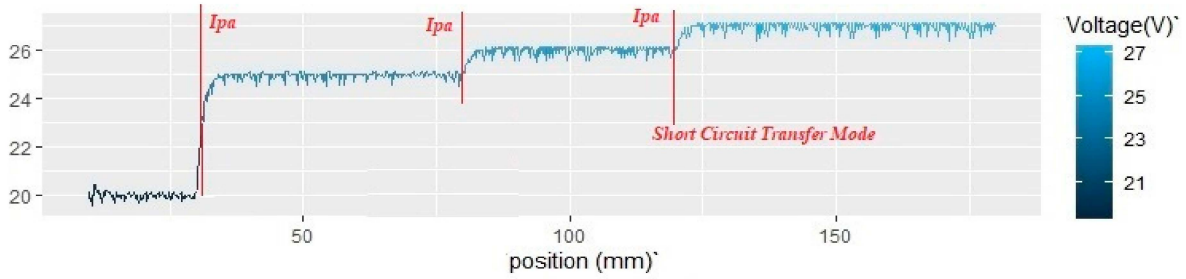


Figure 7. Voltage waveform: Test 1. Ipa: Input parameter alteration (the moment when the input parameters are altered).

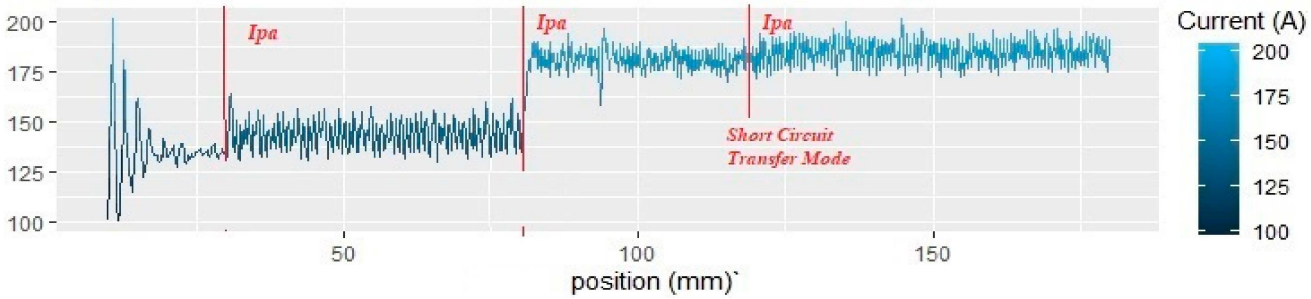


Figure 8. Current waveform: Test 1.

The behavior of the current, voltage, and sound pressure level (SPL) signals exhibited similar patterns. The current was dependent on the voltage supplied to the power source, while the SPL increased in tandem with the rising current, leading to more intense sound pressure levels. It is important to note that in Figure 9, the frequency of peaks during transient current (Ipa) is lower than that observed in the globular transfer mode. However, in the transient current mode, the droplet detaches at a higher speed.



Figure 9. Sound pressure level (SPL): Test 1.

This behavior suggests that in short-circuit transfer mode, material transfer occurs more frequently but with smaller fluctuations in the SPL signal. In contrast, the globular transfer mode is inherently unstable due to the irregular detachment of large droplets, resulting in greater variations in the SPL signal. Consequently, the welding geometry underwent noticeable changes (Figure 10).

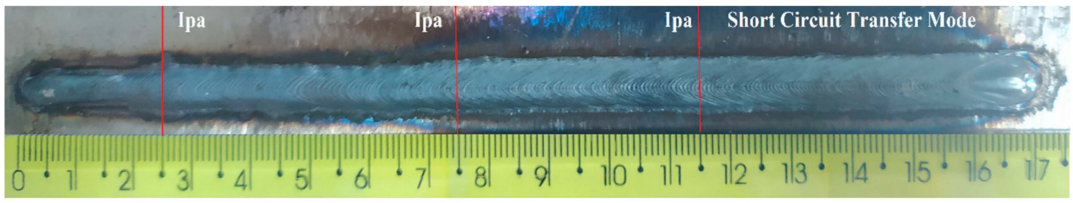


Figure 10. Weld bead geometry: Test 1.

Figures 11 and 12 present the geometric outcomes of the weld bead, corresponding to the conditions discussed above, and should be interpreted in the context of the electrical and acoustic behaviors shown in the preceding figures. Therefore, it is essential to carefully analyze this phenomenon to understand its impact on the overall stability of the welding process. An unstable transfer mode, such as globular transfer, can lead to irregular bead formation, inconsistent penetration, and an increased likelihood of defects, ultimately compromising the mechanical properties of the weld. Understanding these effects is crucial for optimizing welding parameters and ensuring high-quality joints.

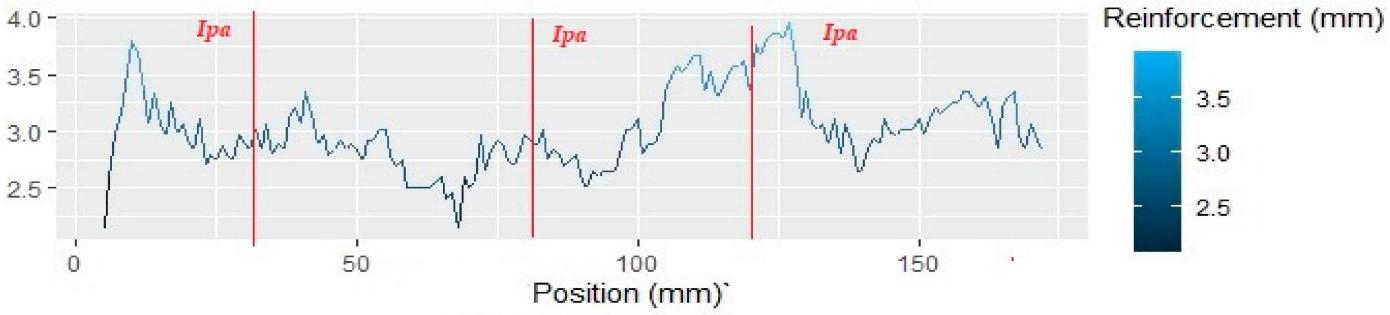


Figure 11. Reinforcement values: Test 1.

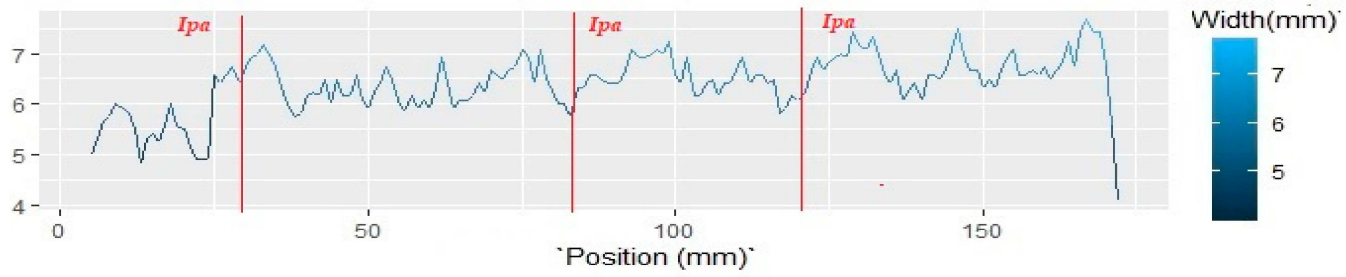


Figure 12. Width values: Test 1.

In this context, Figure 13 provides further insight by showing the transfer mode maps (A) and the droplet detachment frequency map (B). It is evident that the short-circuit transfer mode predominated under the analyzed conditions. Moreover, as the current increases, the droplet detachment frequency also tends to rise, suggesting greater arc stability and improved process efficiency.

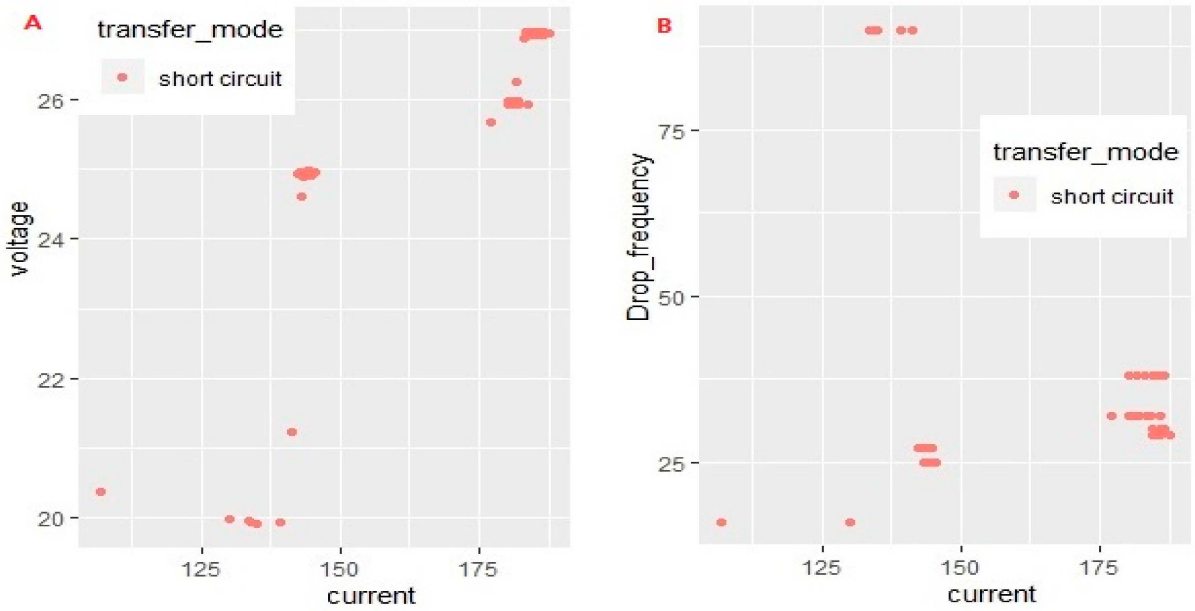


Figure 13. Transfer mode maps (**A**) and detachment frequency map (**B**): Test 1.

In experiment 2, a distinct transition current mode was observed from position 50 to position 100 (as depicted in Figures 14 and 15 respectively.). There was a significant increase in the sound pressure level (SPL) signal, reaching values of 90 dB, indicating a higher intensity of sound generated during this mode (as seen in Figure 16). Additionally, this mode was characterized by fluctuating current values ranging from 180 to 220 A and a constant voltage of 32 V. These fluctuations in current resulted in noticeable changes in the welding geometry, as shown in Figures 17 and 18, respectively.

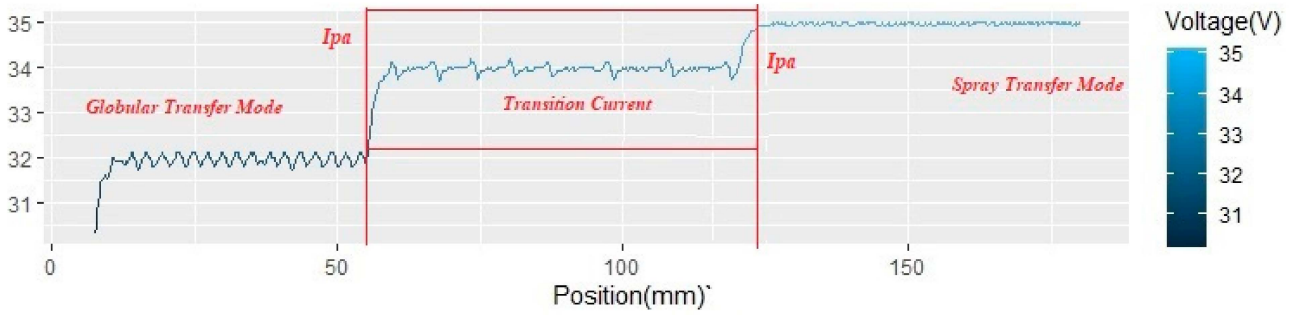


Figure 14. Voltage waveform: Test 2.

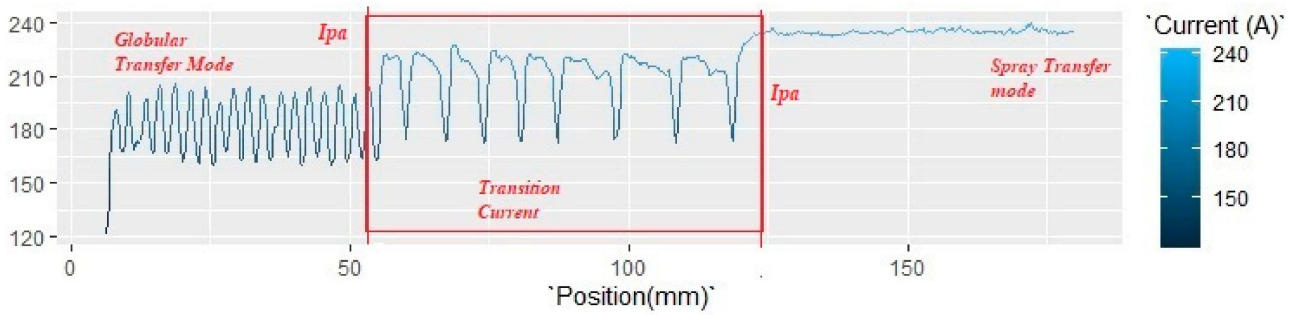


Figure 15. Current waveform: Test 2.

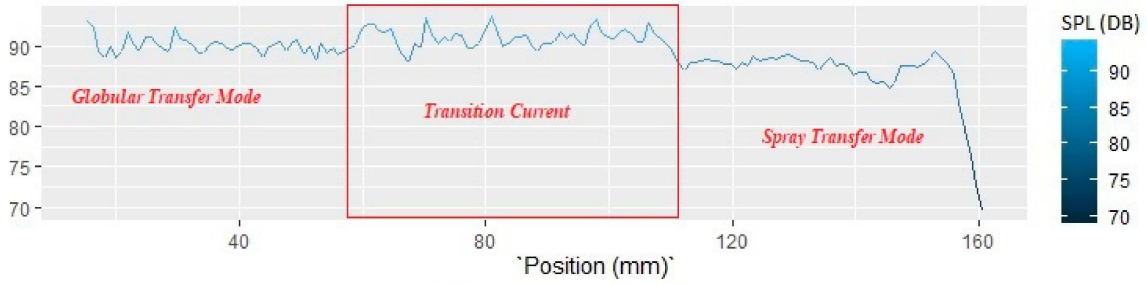


Figure 16. Sound pressure level (SPL): Test 2.



Figure 17. Reinforcement values: Test 2.

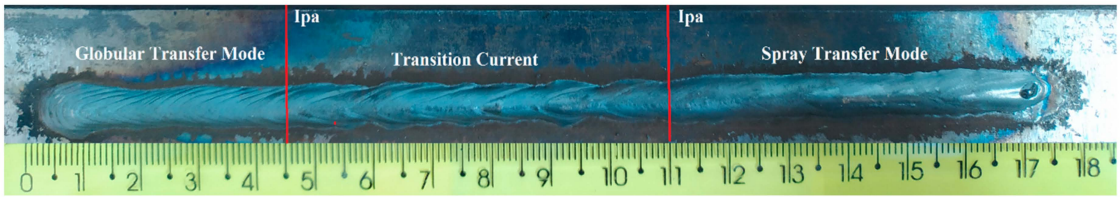


Figure 18. Weld bead geometry: Test 2.

Comparatively, the sound signal for the spray transfer mode exhibited lower decibel levels, with an average of 88 dB. The lower decibel levels suggest a relatively quieter sound produced during the spray transfer mode.

Furthermore, the irregularities observed in the weld bead geometry were particularly prominent in the region associated with the transition current transfer mode (as depicted in Figure 18). These irregularities may be indicative of variations or disturbances in the welding process during this specific mode.

Figures 19 and 20 clearly illustrate the increased metal transfer observed during the experiment. This experiment was designed to vary the wire feed speed, increasing it from 6 to 8 m/min, as shown in the test parameters. Since the wire feed speed directly controls the amount of filler metal supplied, an increase in this parameter naturally results in greater metal deposition. These results confirm that the additional metal transfer and deposition are directly related to the controlled variation in wire feed speed.

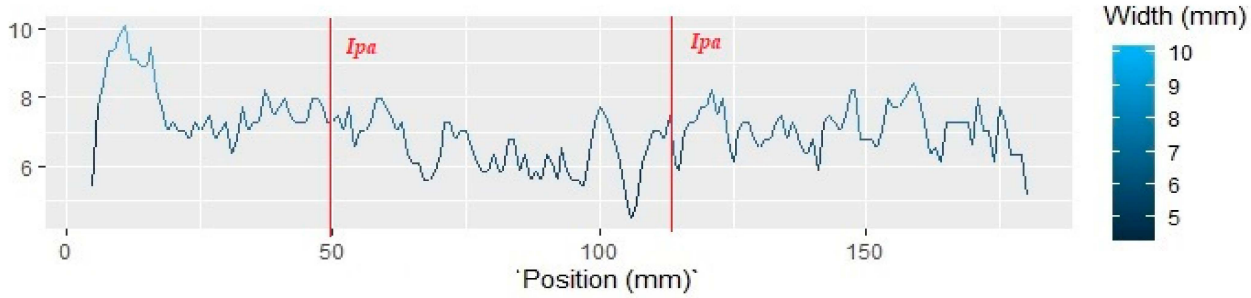


Figure 19. Width values: Test 2.

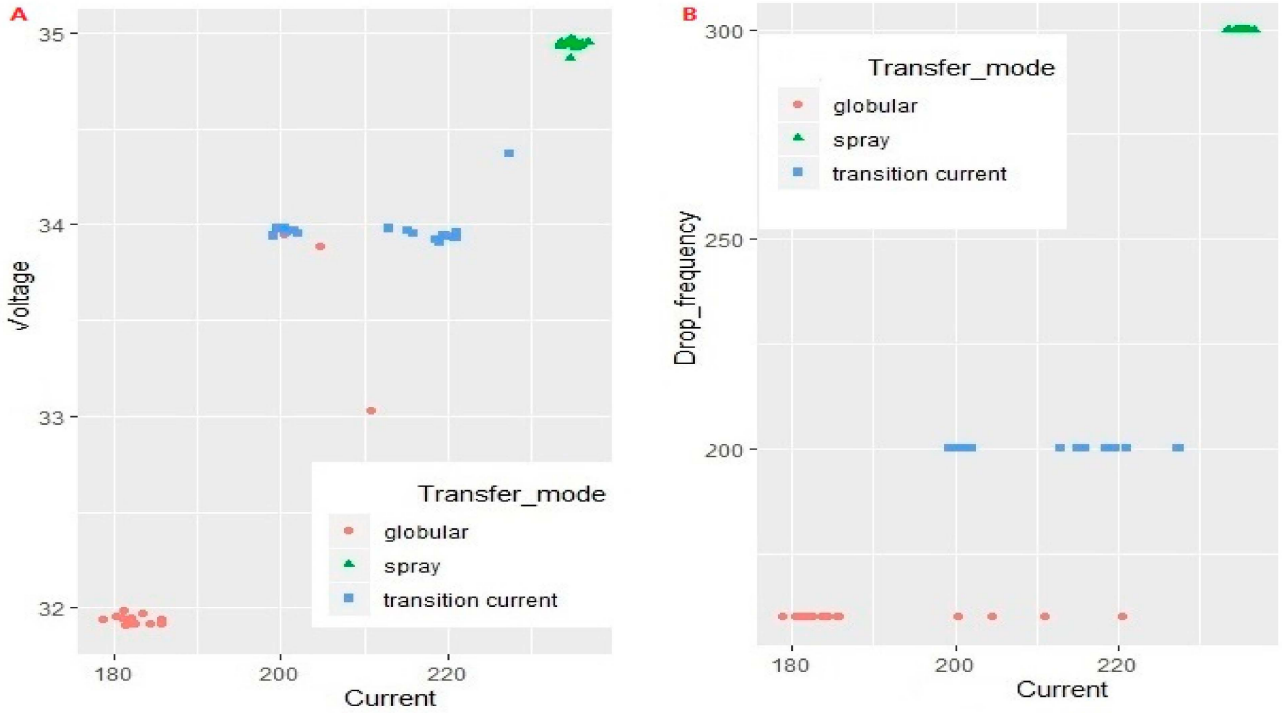


Figure 20. Transfer mode maps (**A**) and detachment frequency map: (**B**) Test 2.

In Experiment 3, an interesting phenomenon was observed when both the wire feed speed and voltage were increased, as illustrated in Figures 21 and 22. The transition current mode exhibited a combination of exploding globular drops and fine spray droplets. This mixture of droplet sizes contributed to the fluctuations observed in the sound signal values, as shown in Figure 23. These variations in the acoustic signal are attributed to the dynamic behavior of droplet detachment during the transition mode.

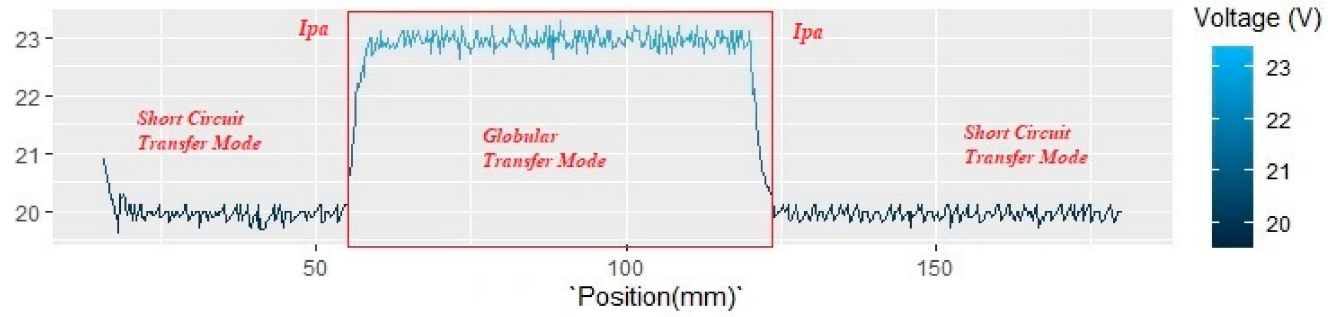


Figure 21. Voltage waveform: Test 3.

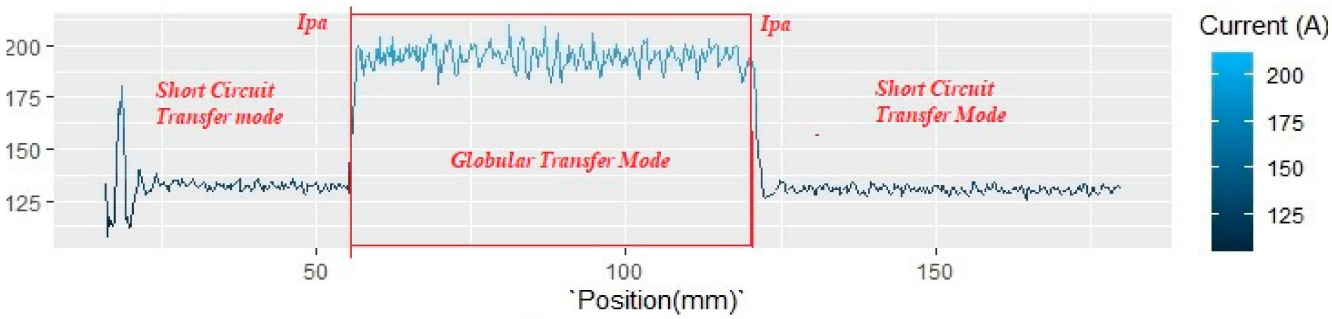


Figure 22. Current waveform: Test 3.

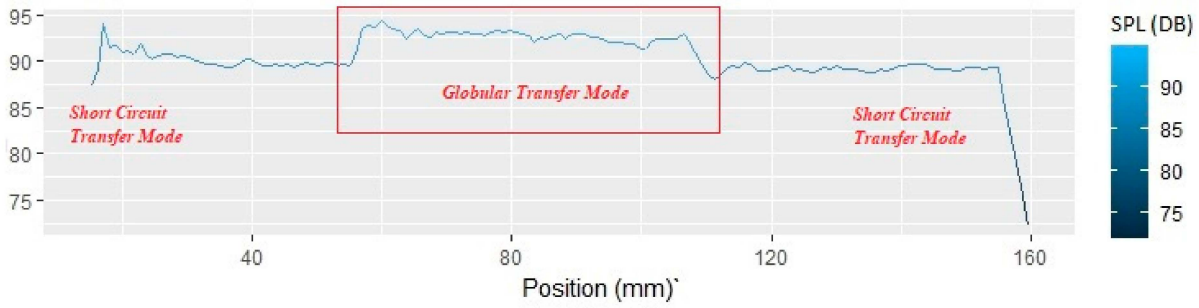


Figure 23. Sound pressure level (SPL): Test 3.

Notably, as the transfer mode shifted toward globular transfer, there was a measurable increase in the sound pressure level (SPL) in decibels. This indicates that globular transfer generates a higher intensity of sound compared to the short-circuit mode. The rise in SPL can be explained by the different droplet detachment mechanisms and the resulting acoustic characteristics inherent to globular transfer.

Overall, the findings suggest that the interaction between current, voltage, and droplet behavior directly influences the transfer mode, which in turn impacts the characteristics of the sound signal. The observations presented in Figure 23 help elucidate the relationship between welding parameters, droplet detachment, and acoustic variations during the process. This transition in transfer mode—from short circuit to globular—led to a marked increase in both material deposition and reinforcement of the weld bead, as demonstrated in Figures 24–26.

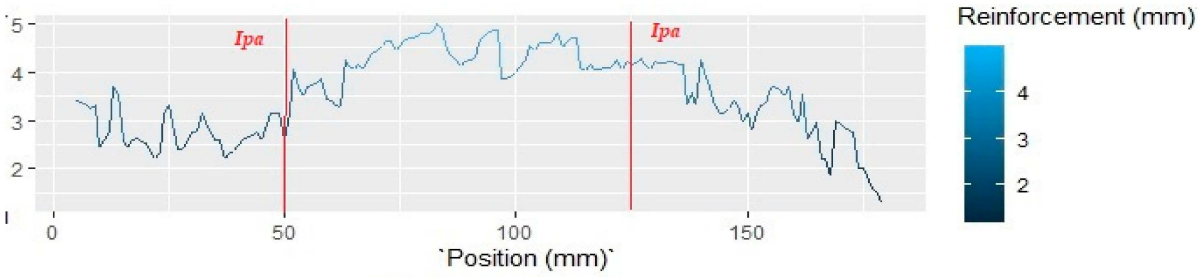


Figure 24. Reinforcement values: Test 3.

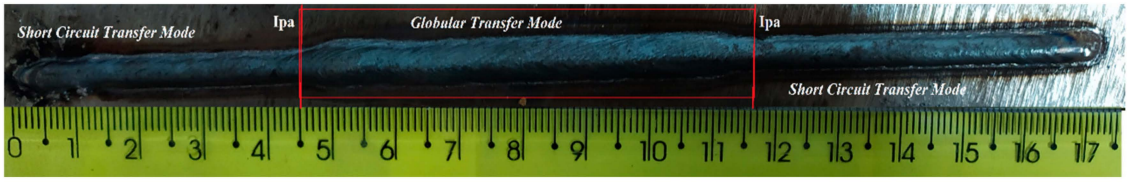


Figure 25. Weld bead geometry: Test 3.

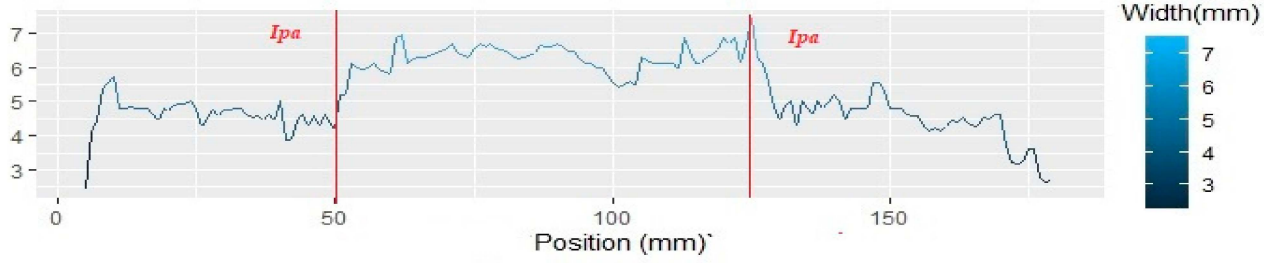


Figure 26. Width values: Test 3.

Taken together, the results of Experiment 3 highlight the significant role of wire feed speed and voltage in affecting the transfer mode, weld bead geometry, and acoustic behavior in the GMAW process.

The two transfer modes identified were globular and short circuit, as shown in Figure 27.

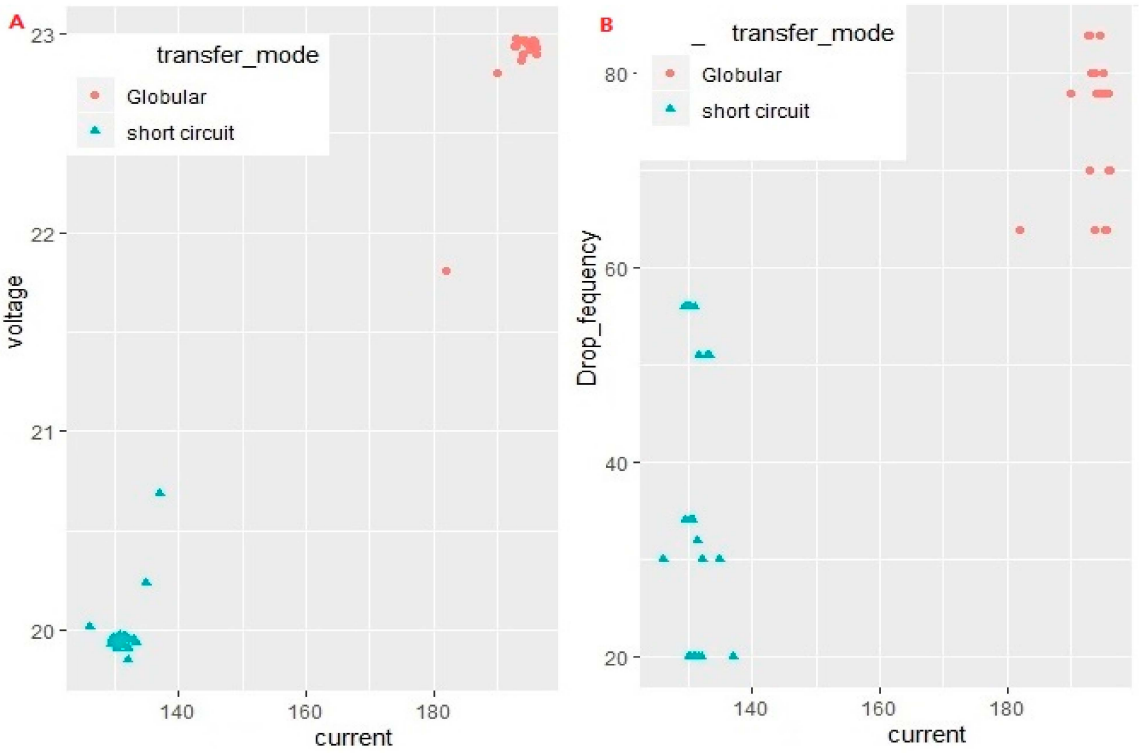


Figure 27. Transfer mode maps (**A**) and detachment frequency map (**B**): Test 3.

Finally, in Test 4, within the voltage range of 22–23 V and current range of 100–150 A (from position 0 to 60 mm), a mixed transfer mode combining both globular and short-circuit characteristics was observed, as demonstrated in Figures 28 and 29. This combination resulted in a high occurrence of splashes, as reflected in the sound pressure level signal as shows in Figure 30.

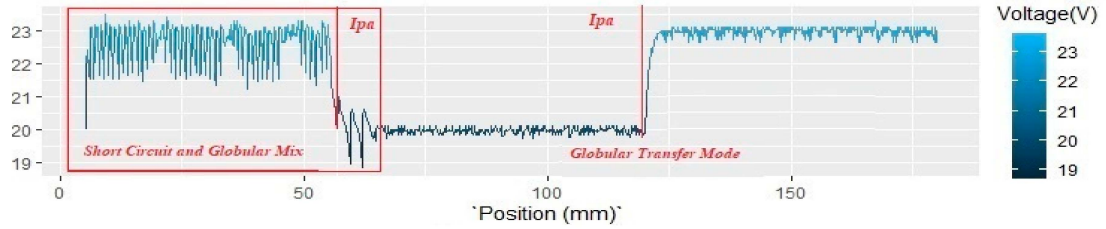


Figure 28. Voltage waveform: Test 4.

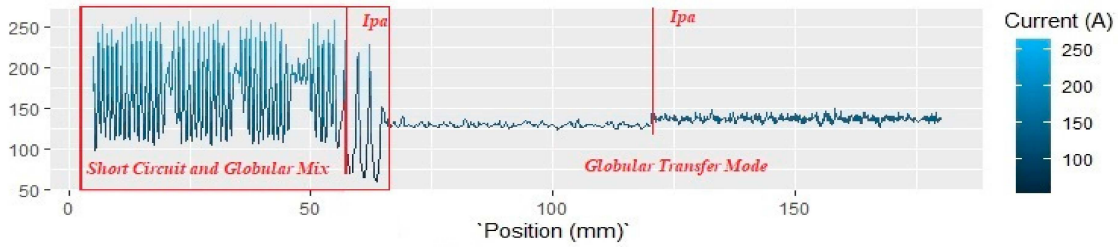


Figure 29. Current waveform: Test 4.

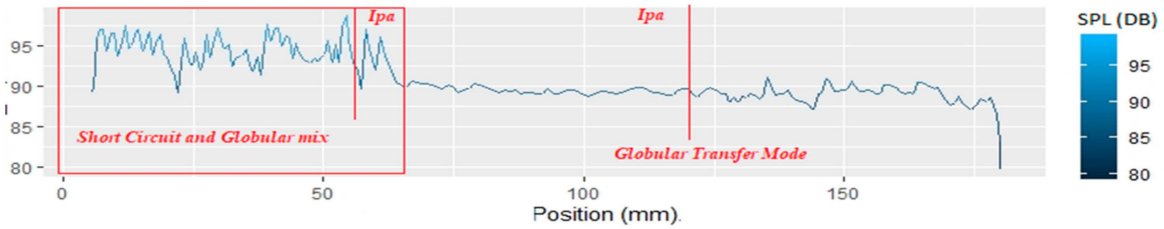


Figure 30. Sound pressure level (SPL): Test 4.

During the initial 60 mm of the weld in experiment 4, it was observed that a decrease in welding speed and an increase in voltage resulted in an irregular welding geometry, as depicted in Figures 31 and 32. Specifically, a welding speed below 8 mm/s was found to cause instability, leading to a highly unstable transfer mode characterized by a mixture of globular and short-circuit transfer.

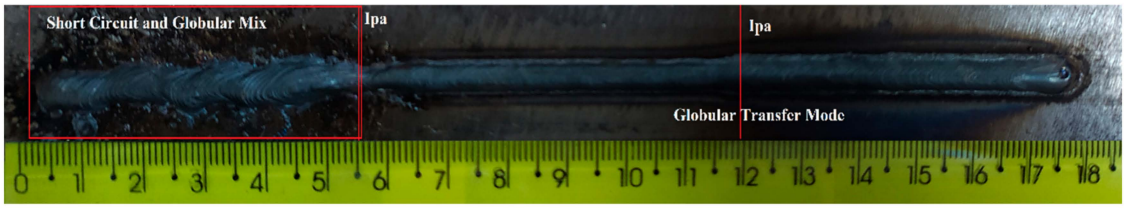


Figure 31. Weld bead geometry: Test 4.

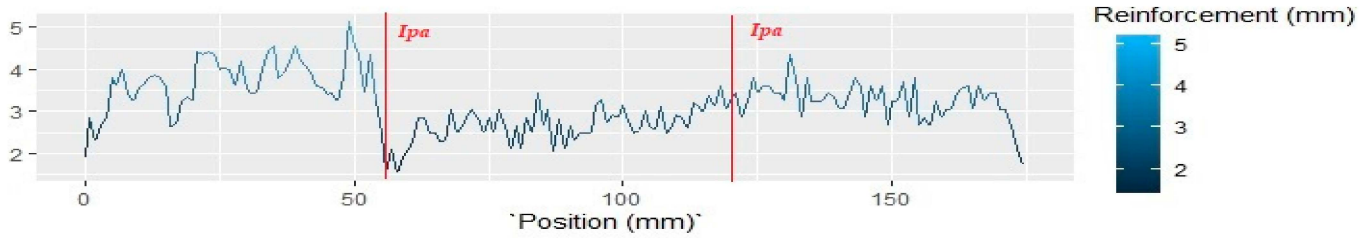


Figure 32. Reinforcement values: Test 4.

Additionally, with a decrease in voltage and an increase in welding speed (positions 60–120), a thinner weld bead was obtained, demonstrate in Figure 33. This suggests that the manipulation of voltage and welding speed influences the geometry of the weld bead.

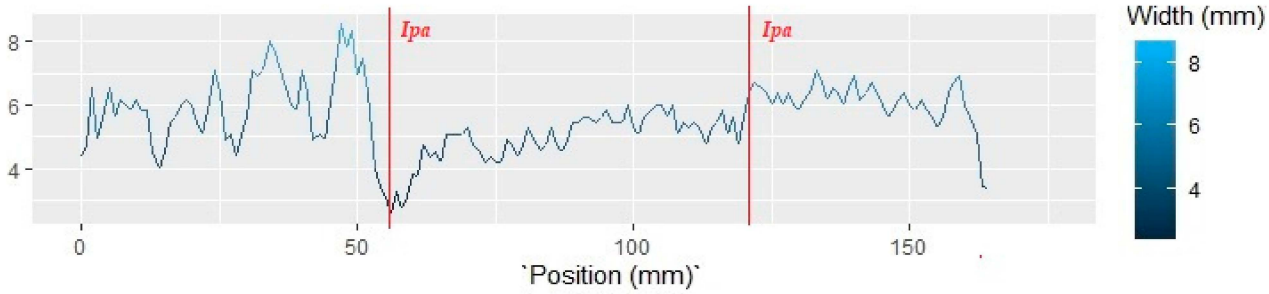


Figure 33. Width values: Test 4.

Overall, the findings from experiment 4 emphasize the impact of welding speed, voltage, and current on the transfer mode, welding geometry, and the occurrence of splashes in the GMAW process.

A mixture of globular and short-circuit transfer modes (transitional current) results in significant spatter, which is reflected in the sound pressure level signal. This transfer mode

occurred due to the low wire feed speed. Additionally, other relationships were identified, such as increased current associated with higher wire feed speeds and greater welding speeds (see Figure 34).

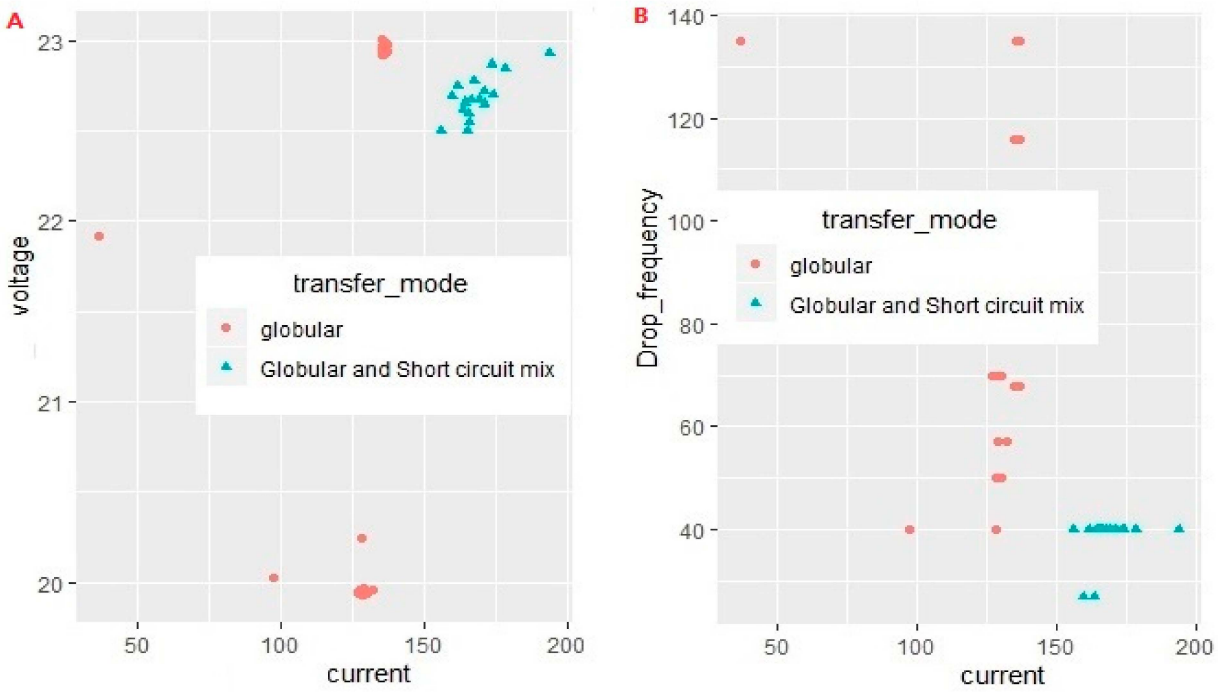


Figure 34. Transfer mode maps (**A**) and detachment frequency map (**B**): Test 4.

The text continues here.

The conducted experiments aimed to identify stable and unstable areas by varying the welding parameters. While the changes in parameters resulted in structural variations in the geometry of the welded bead, it is important to note that irregularities were not necessarily present in all welded sections. Each section underwent individual analysis to assess its stability. The findings and characteristics of the experiments are outlined below.

Table 1 provides a comprehensive overview of the mean and standard deviation values for each calculated parameter. Notably, the standard deviation of sound pressure values exhibited a distinct pattern. As the current increased and changes occurred in the geometry of the weld bead, the standard deviation of sound pressure values consistently decreased. This observation highlights the effectiveness of the sound signal in detecting these changes and its potential as a valuable indicator of welding stability. In particular, the sound signal demonstrated a notable decrease in standard deviation values, often approaching 2, during instances where parameters varied.

Table 1. Statistical Test. A: value of the current (A), V: value of the voltage (V), W: reinforcement of the geometry (mm), W: width of the geometry (mm), and SPL: sound pressure level value (DB).

Position (mm)	SD					Mean				
	A	V	SPL (DB)	W (mm)	R (mm)	A	V	SPL (DB)	W (mm)	R (mm)
					Test 1					
0–30	14.51	0.18	1.00	0.35	0.38	135.57	19.96	90.27	5.46	3.09
30–80	7.57	0.39	1.15	0.48	0.22	143.94	24.86	88.53	6.29	2.79
80–180	6.93	0.53	1.25	0.48	0.34	183.03	26.42	91.13	6.60	3.11

Table 1. *Cont.*

Position (mm)	SD					Mean				
	A	V	SPL (DB)	W (mm)	R (mm)	A	V	SPL (DB)	W (mm)	R (mm)
					Test 2					
0–55	13.61	0.30	1.31	1.30	0.32	183.08	31.85	90.41	8.08	2.62
55–120	21.00	0.99	2.03	0.70	0.36	196.71	32.91	90.36	6.99	2.90
122–180	14.38	0.48	1.25	0.81	0.47	225.08	34.53	88.12	6.88	3.05
					Test 3					
0–55	7.83	0.17	0.99	0.74	0.57	131.8	19.97	90.12	5.05	2.95
55–120	6.25	0.28	1.58	0.57	0.29	193.9	22.89	91.98	6.16	4.38
120–180	6.53	0.29	2.01	0.71	0.69	131.1	20.006	87.93	4.30	2.92
					Test 4					
0–55	44.64	0.55	2.01	1.13	0.62	169.03	22.68	94.41	5.96	3.69
55–120	18.76 (4.81)	0.29	1.54	0.80	0.42	129.64	20.00	89.97	4.89	2.67
120–180	4.17	0.21	1.14	0.73	0.43	136.18	22.93	88.72	6.02	3.24

3.2. Influence of Metal Transfer Modes on Sound Pressure Levels

This section aims to clarify how the decibel levels are affected by the type of metal transfer mode and provide a deeper understanding of the acoustic characteristics associated with each mode.

The spray transfer mode exhibited relatively lower decibel levels, with an average of 88 dB. This suggests that the sound produced during the spray transfer mode is quieter compared to other modes. The reason behind this lower SPL can be attributed to the smaller and more consistent droplet detachment process in this mode, which generates less turbulence and, consequently, a less intense sound.

On the other hand, when transitioning to the globular transfer mode, a significant increase in SPL was observed. In this mode, the decibel levels increased, indicating a higher intensity of sound. The globular transfer mode involves larger droplet detachment, which leads to a more turbulent interaction between the molten metal and the weld pool, thereby producing a more intense sound. The higher SPL is a direct result of the increased energy and larger droplets associated with globular transfer, as opposed to the finer and more controlled droplets of the spray transfer mode.

Additionally, when comparing the sound levels in different phases of the welding process, the decibels recorded during closed-arc conditions—both before the process starts and after it finishes—ranged between 60 and 70 dB. These lower values are consistent with the absence of active metal transfer as the sound generated by the welding arc is minimal in these phases.

In contrast, during open-arc welding, the SPL averaged between 80 and 90 dB, indicating the presence of an active arc and metal transfer. This range is typical of welding processes where the arc is stable but not as turbulent as in modes like globular transfer.

Finally, during moments of high instability in the welding process, the SPL increased significantly, with values reaching up to 94 dB, as observed during Test 4 (positions 5 to 55). These high levels of instability likely correspond to irregular droplet detachment, arc instability, and fluctuations in the molten pool, all of which contribute to a more intense and variable sound signal.

In conclusion, monitoring the decibel levels during welding can provide valuable insights into both the type of metal transfer being used and the occurrence of instability in the process. By tracking the sound intensity, we can identify whether the process is operating in spray or globular transfer mode and, more importantly, pinpoint moments of high instability that could affect the quality of the weld. These findings suggest that acoustic monitoring can be an effective tool for the real-time assessment and optimization of welding processes.

Statistical sequential graphs are presented, illustrating the evolution of key parameters along the welded sections. These include:

bkg_A: background current (A)

pkv_A: peak current value (A)

std_A: standard deviation of the current

mean_A: mean current

m_SPL: mean sound pressure level (dB)

std_SPL: standard deviation of the sound pressure level (dB)

These graphs provide a detailed visualization of how electrical and acoustic signals behave throughout the welding process. The red boxes in the figures highlight regions of instability, characterized by sudden changes in signal behavior and corresponding geometric irregularities in the weld bead, such as lack of fusion and excessive spatter.

It was observed that each welded section tended to reach a state of stability when the welding parameters remained constant. However, when the parameters varied, the sound signal effectively captured these transitions, as indicated by increased standard deviation values—often approaching or exceeding 2 units of standard deviation in the SPL signal (see Figure 35 Std_SPL graph).

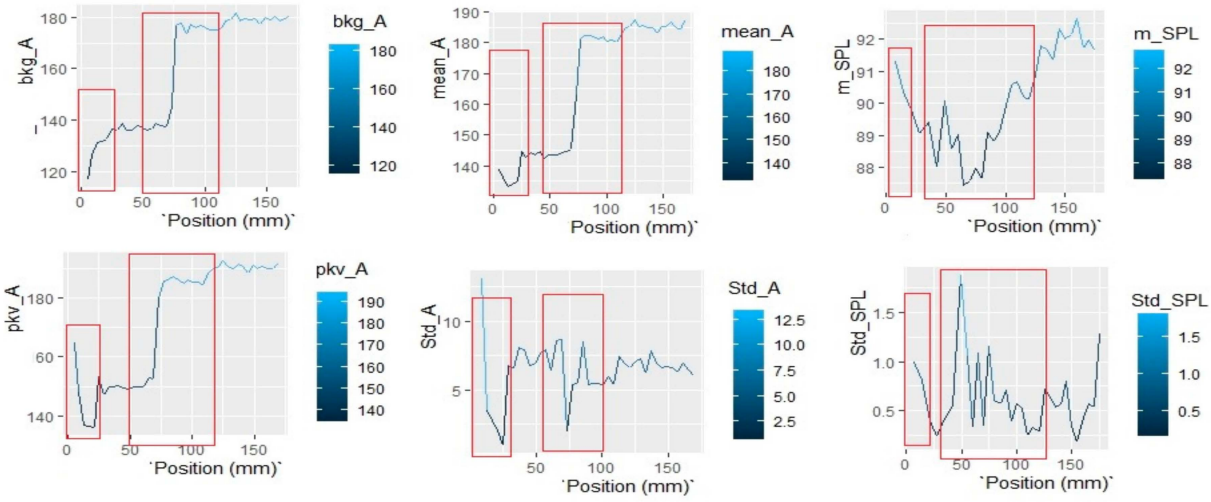


Figure 35. Statistical sequential charts: Test 1.

An interesting observation can be made regarding experiment 2 (Figure 36), where the mean current in the area associated with the transition current exhibited a standard deviation exceeding 20.00. This high standard deviation value, surpassing the threshold of 15, signifies significant variations. Furthermore, an increase in the standard deviation of sound pressure values, approaching two, was indicative of changes in the weld bead's geometry. The subsequent decrease in the SPL graph's values towards the end of the process corresponds to the closing of the arc.

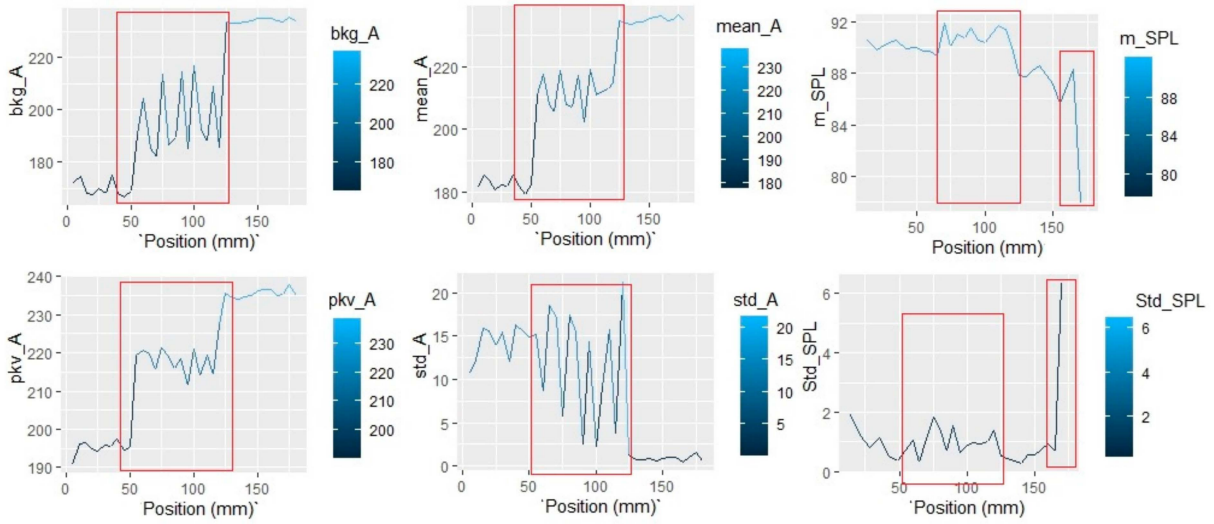


Figure 36. Statistical sequential charts: Test 2.

In experiment 3, a notable trend emerged as the standard deviation for the variables remained relatively low, indicating stable values in the corresponding areas. The observed variations in the sequential graphs presented in Figure 37 were primarily attributed to the fluctuations in voltage and wire feed speed.

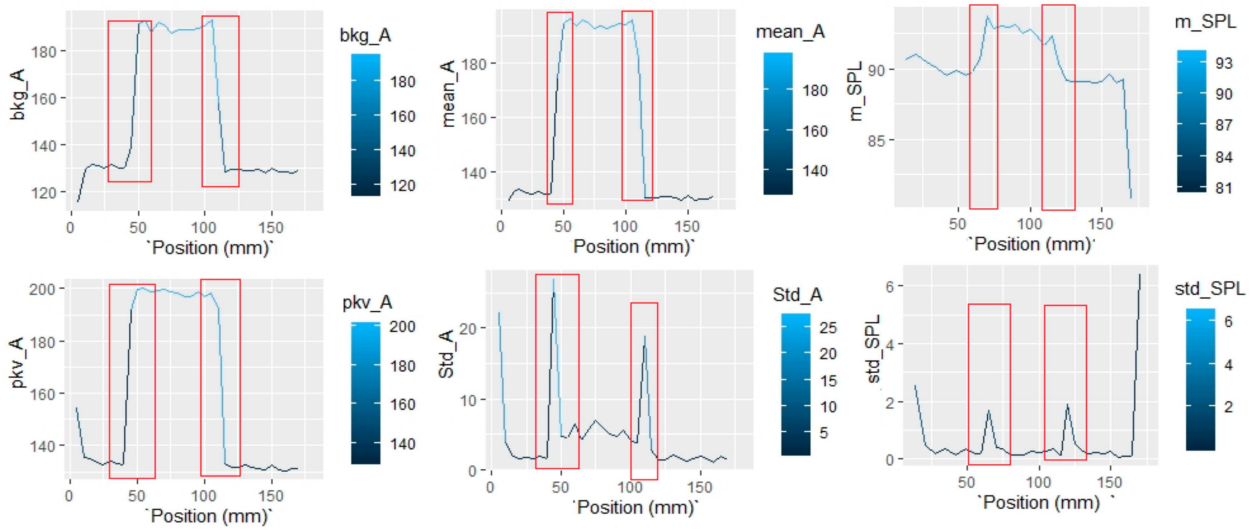


Figure 37. Statistical sequential charts: Test 3.

In Test 4, the statistical signals exhibited irregular patterns, particularly at the positions where transitional current occurred (see the highlighted area in Figure 38). These regions coincide with moments of high instability and are associated with average SPL values of approximately 94 dB—significantly higher than the 80–90 dB typical of stable open-arc conditions, and much higher than the 60–70 dB observed during closed-arc moments before ignition and after the process ends.

In summary, these experimental findings emphasize the importance of analyzing stability states and detecting changes in welding parameters. The sound signal, in particular, proves to be a valuable tool for identifying variations in the welding process and can be used to assess stability and irregularities, with standard deviation values serving as reliable indicators.

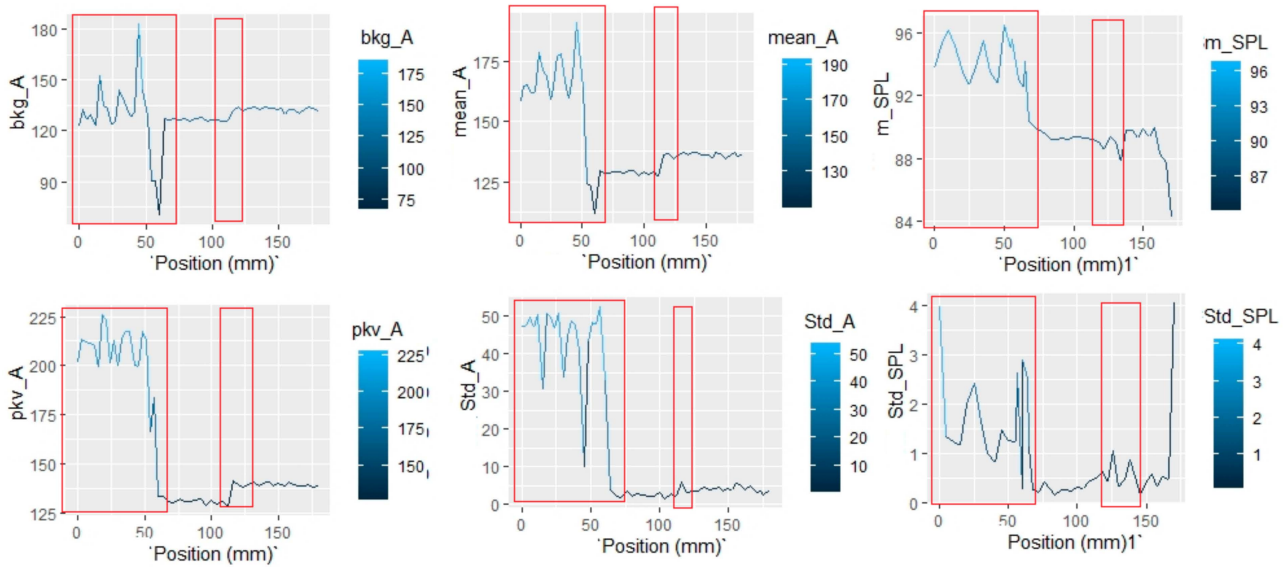


Figure 38. Statistical sequential charts: Test 4.

In conclusion, the statistical indicators—especially the standard deviations of current and SPL—proved to be effective tools for identifying instability in the welding process and correlating electrical and acoustic behavior with weld quality.

The value ranges that cause instability are given in Table 2.

Table 2. Value ranges that cause instability.

Voltage (V)	Welding Speed (mm/seg)	Wire Feed Speed (m/min)
23	7	8
34	12	7

Subsequently, indices proposed in the literature by [8] were calculated (see Figure 39) to support the conclusions obtained in our work. The Transfer Stability Index (TSI) and Transfer Index (TI) were proposed for classifying stability based on the current waveform, while the DCI was based on the voltage waveform. Finally, the Power Ratio (PR) allows for combining current and voltage signal characteristics to monitor stability.

With the results obtained for the calculated indicators, we can conclude that instances of instability can be identified (instability moments highlighted in red). Note that the DCI value reflects the times when changes in the input voltage values were made. For TI, TSI, and PR values, It is possible to identify the moments when changes in the input parameters occur and when transition current zones are present. The transition current is observed in Experiment 2 (positions 55 to 125) and Experiment 4 (positions 0 to 60).

Table 3 summarizes the intervals in which stability and instability are presented in the experiments for each indicator.

Table 3. Intervals in which stability and instability are presented for each indicator.

Status	TI	TSI	DCI	PR
Stable	0–0.10	0.90–1	0–0.2	0.90–1
Unstable	>0.10	<0.90	>0.2	<90

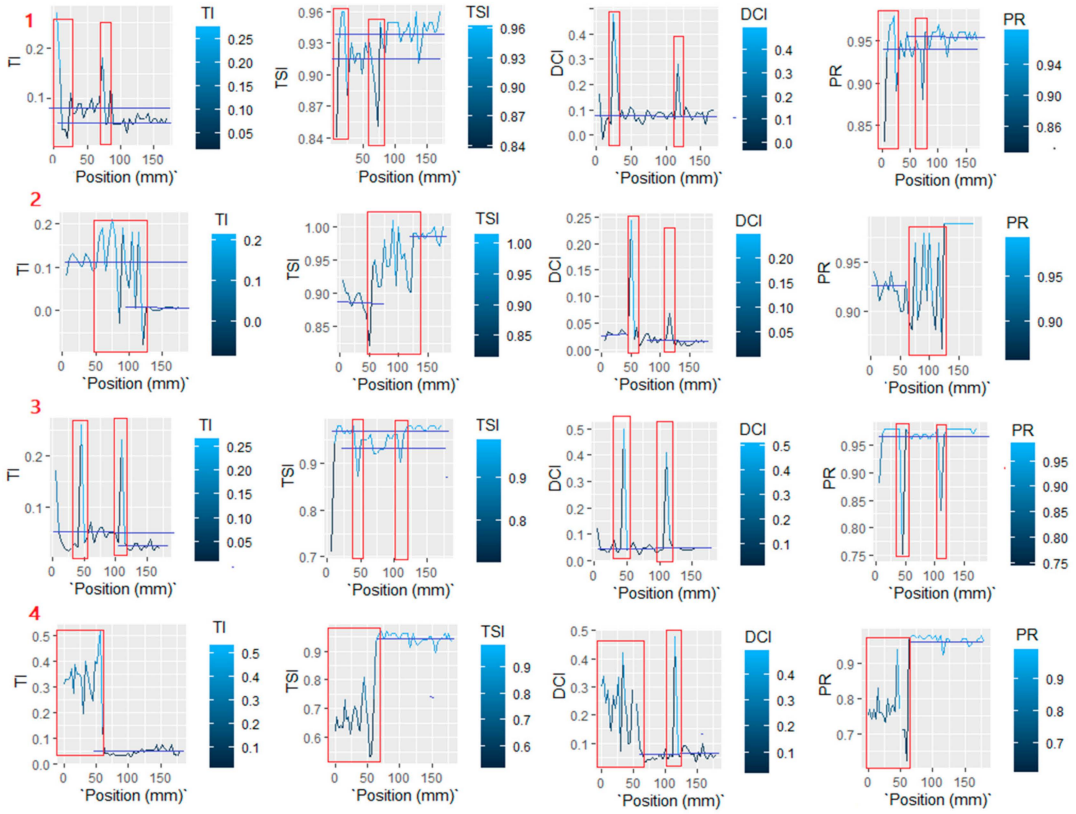


Figure 39. Sequential graphs of TI, TSI, DCI, and PR indicators for each experiment.

The short-circuit and globular transfer modes, in addition to being influenced by the process current and voltage, occur depending on variations in the wire feed speed and welding speed. If we look at the general map of the transfer modes for the four experiments (see Figure 40), the globular and short-circuit transfer modes and the mixture of these two modes can occur in the same ranges of current and voltage. For Test 4, mixed globular and short-circuit transfer modes (transition current) cause a lot of spatters that are reflected in the sound pressure level. This mode of transfer occurred due to the low value of wire feed speed; Therefore, a correlation exists between the two variables.

Taking the transfer mode label as the objective variable, the following conclusions are reached.

The spray transfer mode occurs for current values greater than 231.07 A (in a sample of 53 values, this rule is 100% fulfilled). For values, less than 231 A, the short-circuit transfer mode is presented (441 cases, with a total of 889 values) if the welding speed is greater than 7.5 mm/s, the wire feed speed is less than or equal to 7.6 mm/s, and the voltage is less than or equal to 29.43 V.

For current values less than 231 A and welding speed less than 7.5 mm/s, globular and mixed short-circuit transfer modes are identified (defined in the image as transition current 1). If the welding speed is greater than 7.5 mm/s, the wire feed speed is greater than 7.65 mm/s, and the voltage is greater than 27.5 V, globular transfer occurs (this rule is true for 195 cases in a sample of 204 values).

Considering the SPL variable, the transfer mode identified as a mixture of globular and short-circuit modes (highly unstable) is observed for values greater than 94 dB. The other transfer modes did not reach that value.

To explore these dependencies, the data were integrated, and decision trees were created to separate and classify the data (see Figure 41). The created decision tree was classified with an absolute mean error of 0.243 (see Figure 42).

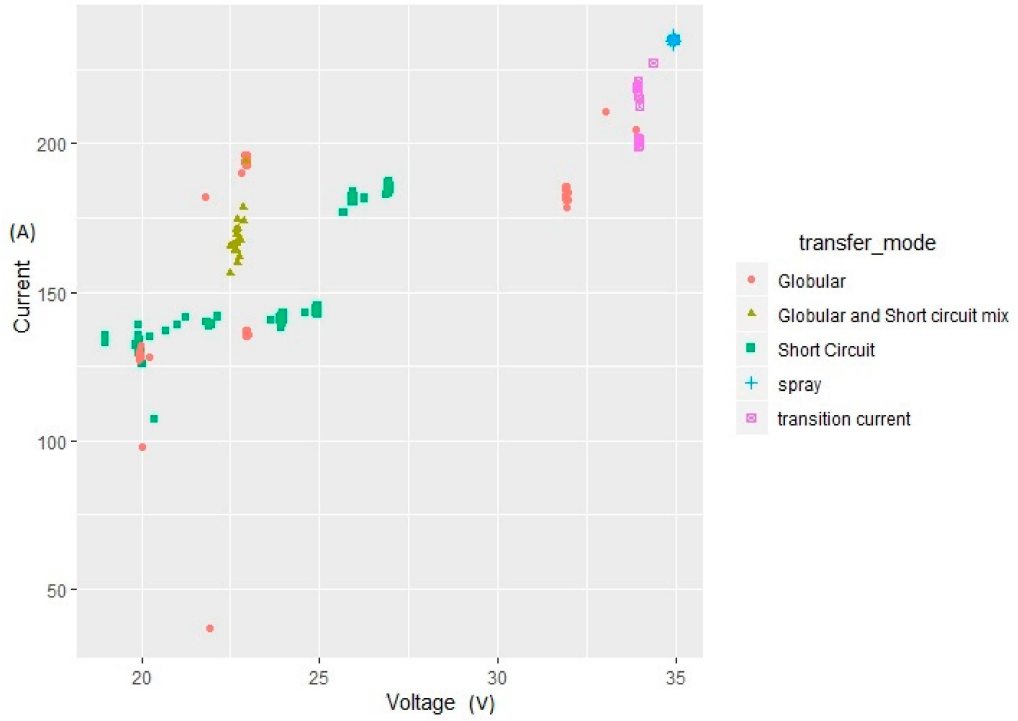


Figure 40. General transfer map (Tests 1–4).

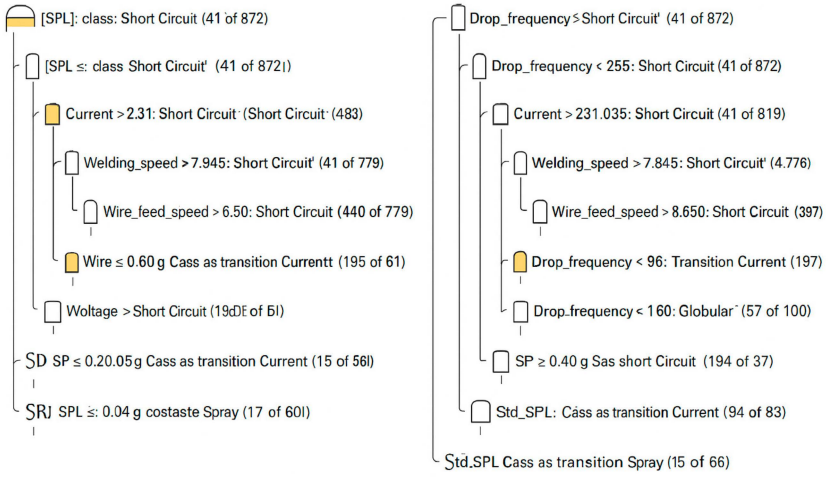


Figure 41. Decision tree for transfer mode classification.

```
R²:                                0.733

Mean absolute error:          0.243

Mean squared error:           0.110

Root mean squared error:  0.332

Mean signed difference:     0.000
```

Figure 42. Decision tree classification error.

Decision trees were implemented with a regression model to establish correlations between numerical values. Regression analysis was performed using the geometry pa-

rameters (reinforcement and width) as the objective variables. The analysis revealed the following insights:

Regarding the reinforcement variable, it was found that when the wire feed speed exceeds 6.81 mm/s, an average reinforcement value of 3.30 mm is obtained. This value is influenced by the welding speed and wire feed speed variables, which are reflected in the SPL values. SPL values greater than 91.95 dB correspond to an average reinforcement of 3.68 mm. Notably, a significant increase in reinforcement is observed when the welding speed exceeds 11 mm/s, reaching an average of 4.18 mm. For SPL values less than 91.95 dB, the average reinforcement is 3.38 mm, with the wire feed speed variable influencing the results. An increase in wire feed speed above 9.4 mm/s leads to a decrease in reinforcement, reaching an average of 2.79 mm. Conversely, wire feed speeds below 6.8 mm/s result in an average reinforcement of 2.4 mm. It is worth mentioning that for currents below 131 A and SPL values below 90 dB, the reinforcement increases to approximately 3.13 mm.

As for the average width, it was found to be 5.75 mm across all four tests. The obtained decision tree revealed a direct association between higher current values (greater than 136 A) and larger width values, with an average width of 6.46 mm. Increasing the wire feed speed also influences the width growth. For wire feed speed values of 7.5 mm/s, an average width of 6.62 mm is observed, while values of 8.4 mm/s with currents below 136 A yield an average width of 5.67 mm.

A stability indicator derived from characteristics extracted from the dataset is proposed.

For training purposes, the following processed values were utilized as inputs: the mean current obtained during the process (mean_A), standard deviation of the current (std_A), peak values of current and voltage (pkv_A and pkv_V, respectively), background values of current and voltage (bkg_A and bkg_V, respectively), and computed metrics such as the Transfer Index (TI), Transfer Stability Index (TSI), Power Ratio (PR), Dip Consistency Index (DCI), mean sound pressure level (m_SPL), standard deviation of sound pressure level (std_SPL), and standard deviation of geometric parameters—reinforcement (std_R) and width (std_W). The network outputs were defined as binary values (0: stable processes, 1: unstable processes).

The stability classification system was developed using Python programming language, employing popular libraries and frameworks for machine learning and neural networks. The system leveraged the capabilities of the TensorFlow library, a widely used open-source platform for building and training neural networks.

For data preprocessing and analysis, the system utilized the NumPy and Pandas libraries, enabling efficient handling and manipulation of numerical data. The OpenCV library was employed for image processing tasks, including image enhancement and feature extraction.

The neural network model was implemented using the Keras API, a high-level neural network library built upon TensorFlow. Keras provides a user-friendly interface for constructing and training neural network architecture.

The training process involved feeding the preprocessed data into the neural network and optimizing the model using techniques such as backpropagation and gradient descent. The model was iteratively adjusted to minimize the classification error and enhance the accuracy of stability predictions.

Throughout the development process, standard practices of machine learning were followed, including data splitting for training and validation, cross-validation, and hyperparameter tuning to optimize the network's performance. Various performance metrics, such as accuracy, precision, and recall, were evaluated to assess the effectiveness of the stability classification system.

Overall, the system combined the power of Python programming language and popular libraries such as TensorFlow, NumPy, Pandas, OpenCV, and Keras to create a robust and efficient solution for stability classification in welding processes.

Data from two new experiments were used to validate the model. In these experiments, the test was conducted with the voltage and current configuration of Test 2 while intentionally subjecting the test specimens to oxidation and paint application to generate irregularities in the GMAW welding process. The presence of paint and rust on the welding surfaces introduces additional complexities and challenges to the welding process. Paint can negatively impact the adhesion of the welding material, resulting in decreased weld quality. Moreover, the emission of gases and particles from the paint during welding can affect the stability of the arc and the overall weld quality. Rust on the welding surfaces can impede the proper fusion of the materials, leading to compromised structural integrity of the weld. By incorporating these intentional irregularities, the model's performance was further evaluated, specifically in its ability to accurately identify and predict issues in the welding process under adverse conditions.

As shown in Figures 43 and 44, a significant change can be observed in the sound level signal when the welding process passes through areas affected by rust and paint. The presence of rust and paint introduces disturbances that impact the welding process. Additionally, the results of current and voltage variations obtained in Test 2 were compared to the results obtained when these disturbances were present. These comparisons allow us to evaluate the effects of rust and paint on the welding parameters and further assess the performance of the model under these challenging conditions.

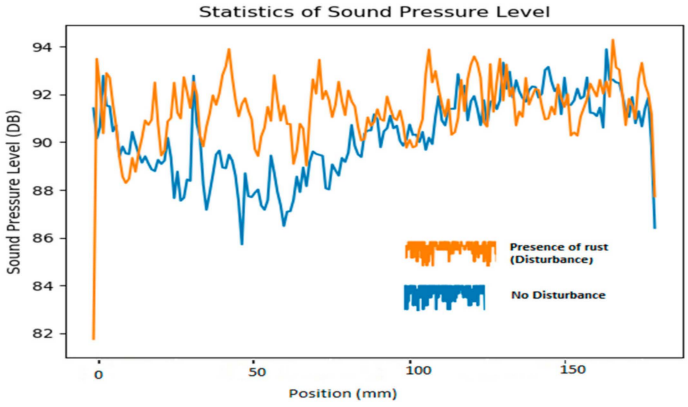


Figure 43. Comparison of Sound pressure signal from Test 2 and Equivalent Test under Disturbance Conditions.

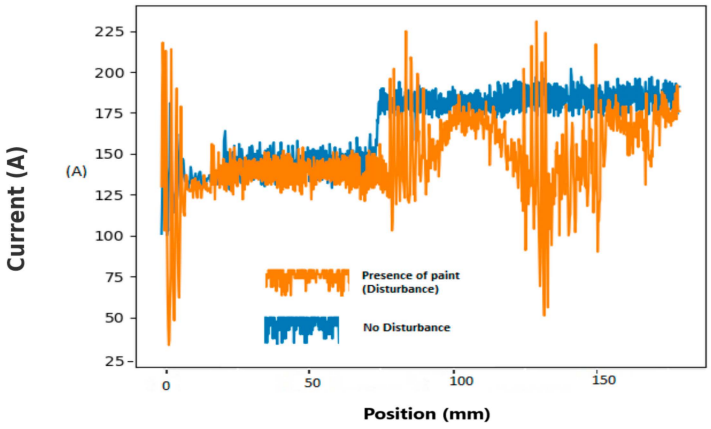


Figure 44. Comparison of Voltage Signals from Test 2 and Equivalent Test under Disturbance Conditions.

Figure 45 illustrates the classification results obtained for all tests based on the calculated indices. The red line represents the stability classification, with a value of 1 indicating unstable areas and a value of 0 indicating moments of stability. It is important to note that there are some values that fall outside the expected range (highlighted in orange in the image), particularly in the DCI parameter. These values were not identified in the model because the experiments involved changes in the reference voltage values supplied to the source. The presence of these out-of-range values highlights the need for further analysis and refinement of the model to account for such variations in the experimental setup.

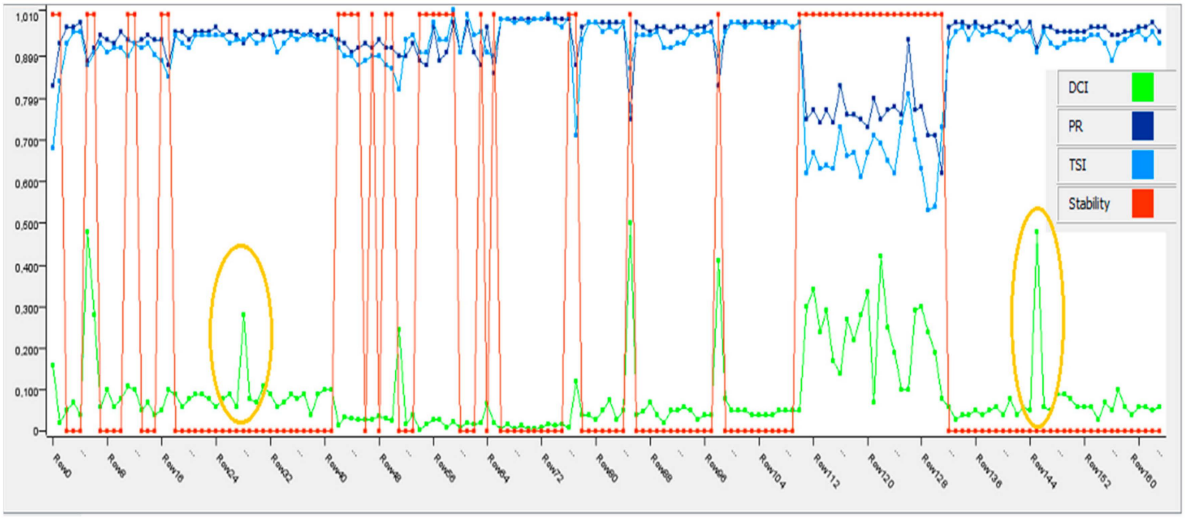


Figure 45. Classification results considering calculated indices and disturbances.

In Figure 46, the pink line represents the prediction obtained from the neural network for the target variable of stability. The neural network's prediction closely aligns with the initial classification line in blue, demonstrating its accuracy. Through the learning process, the model was able to identify areas of instability that were not initially detected in the classification due to the introduced disturbances, as indicated by the regions highlighted in orange. These disturbances, such as oxidation and paint application, had a noticeable impact on the sound pressure signal, and the neural network successfully captured these changes to predict the stability of the welding process.

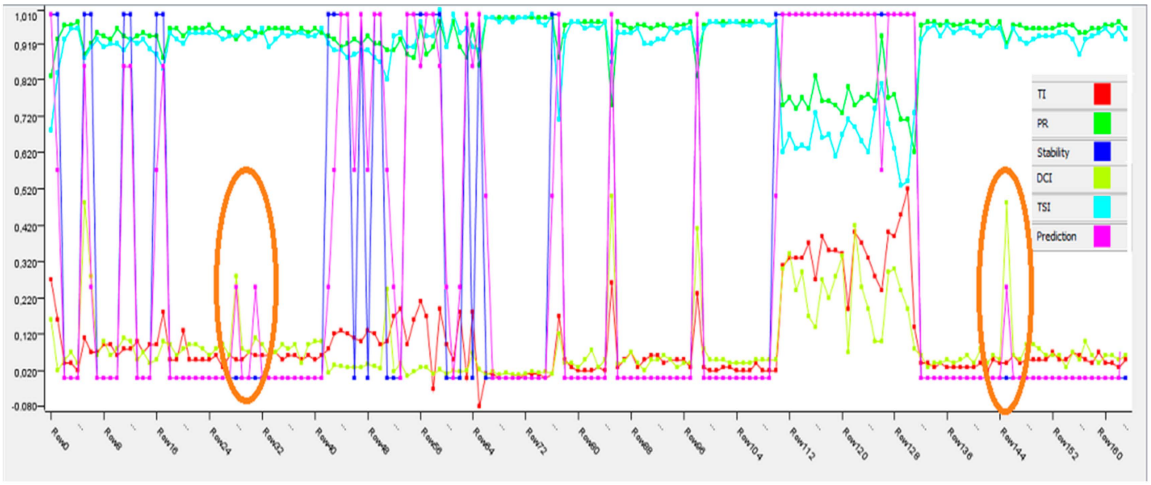


Figure 46. Prediction obtained with the neural network.

4. Conclusions

This study underscores the pivotal role of statistical analysis in classifying and understanding the stability of the GMAW (Gas Metal Arc Welding) process. By leveraging calculated indices such as the Dip Consistency Index (DCI), Power Ratio (PR), Transfer Stability Index (TSI), and Transfer Index (TI), we were able to conduct a detailed and quantifiable evaluation of welding stability. These indices offered invaluable insights into fluctuations and inconsistencies in critical parameters, such as current, voltage, and sound pressure level (SPL), revealing underlying patterns that would otherwise go unnoticed.

The experimental setup was key to obtaining reliable and precise signals for analysis. The meticulously designed welding workstation, coupled with an advanced data acquisition system, ensured a controlled and repeatable environment for collecting data. Through tight control over welding parameters—voltage, current, welding speed, and wire feed speed—we ensured the accuracy and consistency of the data, which in turn strengthened the robustness of our statistical analysis.

A significant finding was the influence of external disturbances—such as oxidation, paints, and other contaminants—on the welding process. These factors notably impacted the SPL signal, with corresponding effects on stability classification. The model we developed was adept at recognizing these instabilities, even when they were not initially anticipated in the dataset. This highlights a key takeaway: the importance of accounting for external variables and their statistical impact in achieving accurate stability assessments.

Our results demonstrate that the fusion of statistical analysis, machine learning techniques, and the careful consideration of external disturbances has enabled a nuanced understanding of stability in the GMAW process. This integrated approach provides an accurate data-driven method for identifying welding instabilities and could lay the foundation for further developments in optimizing welding parameters.

Nevertheless, it is essential to recognize that this study was conducted within a very specific context. The findings should be understood as applicable to a defined set of welding conditions, including a particular electrode diameter, electrode brand, mass of the welded parts, and surface coatings (such as oxides, paints, and dirt). These conditions may not fully represent the broader range of welding scenarios that could arise in other industrial applications. We acknowledge this limitation and emphasize that while the findings offer significant insights, they should be viewed as part of a case study that does not directly extend to all welding processes or materials.

In future work, we aim to expand this research to consider a more diverse set of welding parameters, materials, and surface conditions, which will contribute to a more generalized understanding of welding stability. Furthermore, the methodology presented here can serve as a powerful tool for optimizing welding processes in a variety of industrial contexts, provided the specific parameters are carefully considered.

5. Study Limitations

It is important to note that this study did not include mechanical testing, such as tensile tests, hardness tests, or impact resistance tests, which are essential for comprehensively evaluating the quality and strength of the welds. The decision to exclude these tests was based on the primary focus of the research, which was to analyze the stability of the GMAW welding process through statistical indices and machine learning models.

Although the data presented in this study provide valuable insights into process stability and the classification of metal transfer, the absence of mechanical tests limits the ability to estimate the actual performance of the welds and to determine the optimization of the welding parameters.

We acknowledge that mechanical testing is fundamental for assessing the strength and durability of welds, and this limitation will be addressed in the revised version of the article. In future studies, we plan to include mechanical tests to complement the presented data and provide a more holistic understanding of the relationship between process stability and weld strength.

6. Future Research Directions

Finally, other techniques exhibiting high accuracy for stability analysis that could be developed in the future include 3D computational modeling, simulations, spectroscopy, spectral analysis, and X-ray observation systems.

Author Contributions: All authors contributed significantly to this work. E.M.M.P. conceptualized and designed the research, conducted the data analysis, and drafted the manuscript. G.A.B. supervised the experimental procedures and provided critical revisions to the manuscript. S.C.A.A. served as advisors and reviewers, offering guidance on the research methodology, statistical analysis, and manuscript improvement. All authors have read and agreed to the published version of the manuscript.

Funding: This work has been supported by the University of Brasília (UnB), the government research CAPES foundation, and CNPq.

Data Availability Statement: The data collected during the research are available in the repository Open Science Framework (OSF) and can be accessed at https://osf.io/j2swb/ (accessed on 25 March 2025). Any additional data or materials related to this study will be made available upon reasonable request.

Conflicts of Interest: The authors declare no conflicts of interest.

References

1. Adolfsson, S.; Bahrami, A. On-line quality monitoring in short-circuit gas metal arc welding. *Weld. J.* **1999**, *78*, 02_s59.
2. Luksa, K. Influence of weld imperfection on short circuit GMA welding arc stability. *J. Mater. Process. Technol.* **2006**, *175*, 285–290. [CrossRef]
3. Anzehaee, M.M.; Haeri, M. Estimation and control of droplet size and frequency in projected spray mode of a gas metal arc welding (GMAW) process. *ISA Trans.* **2011**, *50*, 409–418. [CrossRef] [PubMed]
4. Suban, M. Determination of stability of MIG/MAG welding processes. *Qual. Reliab. Eng. Int.* **2001**, *17*, 345–353. [CrossRef]
5. Alfaro, S.C.A.; Cayo, E.H. Sensoring fusion data from the optic and acoustic emissions of electric arcs in the GMAW-S process for welding quality assessment. *Sensors* **2012**, *12*, 6953–6966. [CrossRef] [PubMed]
6. Kang, M.; Kim, Y.; Ahn, S.; Rhee, S. Spatter rate estimation in the short-circuit transfer region of GMAW. *Weld. J.* **2003**, *82*, 238s–247s.
7. Bestard, G.A.; Sampaio, R.C.; Vargas, J.A.; Alfaro, S.C.A. Sensor fusion to estimate the depth and width of the weld bead in real time in GMAW processes. *Sensors* **2018**, *18*, 962. [CrossRef] [PubMed]
8. Ogunbiyi, B.; Norrish, J. Monitoring indices for metal transfer in the GMAW process. *Sci. Technol. Weld. Join.* **1997**, *2*, 33–35. [CrossRef]

Disclaimer/Publisher's Note: The statements, opinions and data contained in all publications are solely those of the individual author(s) and contributor(s) and not of MDPI and/or the editor(s). MDPI and/or the editor(s) disclaim responsibility for any injury to people or property resulting from any ideas, methods, instructions or products referred to in the content.